Turun yliopisto
University of Turku

ATOMIC SCALE ENGINEERING AND UNDERSTANDING OF NOVEL INTERFACES BETWEEN OXIDE FILMS AND SEMICONDUCTOR CRYSTALS

Muhammad Yasir

University of Turku

Faculty of Mathematics and Natural Sciences
Department of Physics and Astronomy

Supervised by

Docent Pekka Laukkanen
Department of Physics and Astronomy
University of Turku
Turku, Finland

Ph.D. Mikhail Kuzmin
Ioffe Physical-Technical Institute
St. Petersburg
Russian Federation

Docent Marko Punkkinen
Department of Physics and Astronomy
University of Turku
Turku, Finland

Reviewed by

Associate Professor Hele Savin
Department of Micro- and Nano Science
Aalto University
Helsinki, Finland

Associate Professor Christopher Hinkle
Department of Mat. Sci. and Eng.
University of Texas at Dallas
Dallas, United States

Opponent

Professor Greg Hughes
School of Physical Sciences,
Dublin City University,
Dublin, Ireland

Contents

Acknowledgement

Firstly, I would truly like to thank and express my sincere gratitude to my supervisor Docent Pekka Laukkanen, for giving me an opportunity to work in the Materials Physics group. Also I appreciate his guidance, help, advice, support and sharing of his immense knowledge throughout my research studies.

I would also like to thank to my co-supervisor Dr. Mikhail Kuzmin. While working with him, I have learnt a lot from his advice and understanding about the subject. I really admire of his calmness and deep insight on the subject. I would also like to mention my second co-supervisor Docent Marko Punkkinen. This is very inspiring how hard he works for long hours throughout the day without taking long breaks and still shows a very good sense of humor. It is very impressive that how he manages to combine his interest in philosophy and music along with Physics. My sincere thank goes to Professor Kalevi Kokko. His precious support was always there whenever it was needed. He always showed a very welcoming attitude whenever I approached him on different matters. I also wish to thank to my lovely labmates Dr. Johnny Dahl, M. Sc. Marjukka Tuominen, M. Sc. Jaakko Mäkelä, M. Sc. Henrik Levämäki, Dr. Jouko Lång, Dr. Marja Ahlola and Veikko Tuominen. All of them have been very supportive and helpful. It was a pleasant experience to work with them. Special thanks to M. Sc. Jaakko Mäkelä and M. Sc. Marjukka Tuominen for always being very warm and friendly to me. In particular, I am grateful to my fellow friend Dr. Johnny Dahl for sharing his views in our unforgettable long and thoughtful conversations beside our lab work. I really praise his knowledge on diverse topics. He has always been extremely supportive whenever I have needed his valuable suggestions and fruitful advises.

Last but not least, I would like to thank my dear parents and cute siblings for their love and prayers for me. They have always supported me on my decisions and never let me feel that I am living far away from them.

Abstract

Surface properties of semiconductor crystals play a significant role in the operation of different devices like transistors, LEDs, and solar cells. For better performance of the devices, it is essential to minimize the amount of harmful surface and interface defects. For example, control over the oxygen induced defects is difficult during deposition of any film (e.g., metal oxide films) on a semiconductor crystal. On the other hand, tailoring and characterization of the semiconductor interfaces is not an easy task due to the buried nature of these structures.

In this thesis, we have studied the effect of different adsorbates (Sr, Ba, Si, and Sb) and metal oxides (BaO, SiO_2, Al_2O_3 and Sb_2O_3) on different semiconductor surfaces: Si(100), Ge(100) and GaAs(100). In this experimental work, several complementary characterization methods were used including low energy electron diffraction (LEED), synchrotron-radiation photoemission spectroscopy (SR- PES) and scanning tunneling microscopy (STM). These results were interconnected to capacitance-voltage (CV) and photoluminescence (PL) measurements via collaboration with other research groups.

The results can be summarized as follows: It is demonstrated the reduction in the defects amount at Al_2O_3/GaAs interface when an intermediate thin layer of BaO was deposited before atomic layer deposition of Al_2O_3. In the case of epitaxial BaO/SiO_2 system, the crystallinity of the interface even after the incorporation of significant amount of oxygen atoms into Si is an interesting finding. It is also evident in this research that metal interaction with semiconductor substrate can also induce degradation in the interface. This degradation can be avoided with the modification of starting surface and by adopting a specific procedure for oxide film growth. Furthermore, a growth of crystalline Sb_2O_3 film has been also presented by careful consideration of deposition temperature and time.

Tiivistelmä

Kiteisten puolijohdepintojen ominaisuudet vaikuttavat merkittävästi erilaisten laitteiden kuten transistoreiden, LED:ien ja aurinkokennojen toimintaan. Olennainen osa näiden laitteiden tehokkuuden parantamista on erilaisten haitallisten pinta- ja rajapintavirheiden minimointi. Esimerkiksi hapen aiheuttamia virheitä on vaikea kontrolloida kasvatettaessa mitätahansa ohutkalvoa (esim. metallioksidikalvot) kiteisen puolijohteen päälle. Toisaalta puolijohderajapinnat ovat luonteensa takia hankalia mallintaa ja karakterisoida, koska ne pinnan alla (hautautuneita).

Tässä väitöskirjassa olemme tutkineet miten eri absorbaatit (Sr, Ba, Si ja Sb) ja metallioksidit (BaO, SiO_2, Al_2O_3 ja Sb_2O_3) reagoivat erilaisilla puolijohdepinnoilla: Si(100), Ge(100) ja GaAs(100). Tässä kokeellisessa teoksessa yhdistettiin useita karakterisointimenetelmiä mukaanlukien matalaenergisten elektronien diffraktio (LEED), synkrotronifotoelektronispektroskopia (SR- PES) ja tunnelointimikroskopia (STM). Näistä mittausmenetelmistä saadut tulokset yhdistettiin kapasitanssi-jännite (CV) ja fotoluminesenssi (PL) mittauksiin, jotka suoritettiin yhteistyössä muiden tutkimusryhmien kanssa.

Tutkimuksemme tulokset voidaan tiivistää seuraavasti: Haitallisten virheiden määrää voidaan vähentää Al_2O_3/GaAs rajapinnalla lisäämällä ohut kalvo bariumoksidia (BaO) substraatin päälle ennen alumiinioksidin atomikerroskasvatuksta. Järjestäytyneen BaO/SiO_2 -systeemin tapauksessa on mielenkiintoista huomata, että rajapinta on kiteinen, vaikka pii sisälsi huomattavan määrän happiatomeja. Tässä tutkimuksessa on myös osoitettu, että metallin ja puolijohteisen substraatin vuorovaikutuksen seurauksena tapahtuu rajapinnan laadullista heikkenemistä. Tätä rappeutumista voidaan välttää muokkaamalla substraatin pintaa ja ottamalla käyttöön tietynlainen menetelmä oksidikalvon kasvatuksessa. Tämän lisäksi kiteisen Sb_2O_3 kalvon kasvatustapa on myös esitelty kiinnittämällä suurta huomiota kasvatuslämpötilaan ja -aikaan.

List of Publications

The content of this thesis is based on following five research articles. I contributed in sample preparations, PES, LEED and STM measurements and data analysis for all of these articles. For paper 1 and paper 5, I was the responsible for writing the manuscript.

1) **M. Yasir**, J. Dahl, M.Kuzmin, J. Lång, M. Tuominen, M. P. J. Punkkinen, P.Laukkanen, K. Kokko, V.-M. Korpijärvi, V. Polojärvi and M. Guina: *Growth and properties of crystalline barium oxide on the GaAs(100) substrate*. Applied Physics Letters 103, 191601 (2013).

2) M. Kuzmin, P. Laukkanen, M.P.J. Punkkinen, **M. Yasir**, M. Tuominen, J. Dahl, J. Lång and K. Kokko: *Atomic structure and thermally induced transformation of the crystalline BaO/Si(100) junction. Physical Review B 90, 235405 (2014).*

3) M. Kuzmin, P. Laukkanen, **M. Yasir**, J. Mäkelä, M. Tuominen, J. Dahl, M. P. J. Punkkinen, K. Kokko, H.-P. Hedman, J. Moon, R. Punkkinen, V. Poloj¨arvi, V.-M. Korpij¨arvi, and M. Guina: *Observation of unusual metal-semiconductor interaction and metal-induced gap states at an oxide-semiconductor interface: The case of epitaxial BaO/Ge(100) junction,* Physical Review B 92, 165311, (2015).

4) M. Kuzmin, P. Laukkanen, M. P. J. Punkkinen, J. Mäkelä, **M. Yasir**, J. Dahl, M. Tuominen, and K. Kokko, *Towards the atomically abrupt interfaces of SiO_x / semiconductor junction. Advanced Materials Interfaces (2016).* DOI: 10.1002/admi.201500510.

5) **M.Yasir**, M. Kuzmin, M.Punkkinen, J. Mäkelä, M. Tuominen, J. Dahl, P. Laukkanen and K. Kokko. *Synthesis and Properties of Crystalline Thin Film of Antimony Trioxide on the Si(100) Substrate.* Applied Surface Science 349 (2015), 259-263.

The following articles where I contributed but these are not included in my doctoral thesis.

1. P. Laukkanen, J. Lång, M. Punkkinen, M.Kuzmin, M. Tuominen, **M. Yasir**, J. Dahl, V. Yuominen, K. Kokko, V. Polojärvi, J. Salmi, V. M. Korpijärvi, A. Aho, A. Tunkiainen, M. Guina, H. P. Hedman and R. Punkkinen: *Synthesis and Characterization of Monocrystalline Tin-Oxide Thin Films on III-V Compound Semiconductor*. Advanced Materials: Interfaces 12/2013. Published only online. DOI:10.1002/admi.20130002.

2. *M. P. J. Punkkinen, P. Laukkanen, M. Kuzmin, H. Levämäki, J. Lång, M. Tuominen,* **Y. Zaki**, *J. Dahl, S. Lu, E. Delczeg-Czirjak, L. Vitos and K. Kokko: Does Bi form clusters in $GaAs_{1-x}Bi_x$ alloys ?Semiconductor Science and Technology 29. (2014).*

3. *M. Tuominen, J. Lång, J. Dahl, M. Kuzmin,* **M. Yasir**, *J. Mäkelä, J. Osiecki, K. Schulte, M. Punkkinen, P. Laukkanen and K. Kokko: Oxidized crystalline (3×1)-O surface phases of InAs and InSb studied by high-resolution photoelectron spectroscopy.* Applied Physics Letters 106, 011606 (2015).

4. M. Tuominen, **M. Yasir**, J. Lång, J. Dahl, M. Kuzmin, M. P. J. Punkkinen, P. Laukkanen, K. Kokko, K. Schulte, V.-M. Korpijärvi, V. Polojärvi and M. Guina: *Oxidation of GaAs semiconductor at Al_2O_3/GaAs junction.* Physical Chemistry Chemical Physics, 02/2015. Published only online DOI: 10.1039/c4cp05972g.

5. J. Mäkelä, M. Tuominen, Kuzmin, **M. Yasir**, J. Lång, J. Dahl, M. P. J. Punkkinen, P. Laukkanen, K. Kokko, K. Schulte and R. M. Wallace: *Line shape and composition of*

the In3d core-level photoemission for the interface analysis of In-containing III-V semiconductors. Applied Surface Science 329, 371 (2015).

6. J. Mäkelä, M. Tuominen, **M. Yasir**, V. Polojärvi, A. Tukiainen, M. Kuzmin, M.P.J. Punkkinen, P. Laukkanen, K. Kokko and M. Guina. Effects of *Thinning of AlInP epilayer for TiO$_2$-AlInP junctions,* Journal of Electron Spectroscopy and Related Phenomena 205 (2015), 6- 9.

7. J. Mäkelä, M. Tuominen, **M. Yasir**, M. Kuzmin, J. Dahl, M. P. J. Punkkinen, P. Laukkanen, K. Kokko, and R. Wallace. *Oxidation of GaSb(100) and its control studied by scanning tunneling microscopy and spectroscopy.* Applied Physics Letters, 107, 061601 (2015).

8. M. Kuzmin, P. Laukkanen, M. P. J. Punkkinen, J. Mäkelä, **M. Yasir**, J. Dahl, M. Tuominen, and K. Kokko. *Sr/Si(100)(1×2) reconstruction as a template for the growth of crystalline high-k films on silicon: Atomic structure and reactivity.* (Available online Surface Science, 1st August, 2015).

9. M.P.J. Punkkinen, A. Lahti, P. Laukkanen, M. Kuzmin, M. Tuominen, M. Yasir, J. Dahl, J. Mäkelä, H.L. Zhang, L. Vitos, K. Kokko, *Thermodynamics of the pseudobinary GaAs$_{1-x}$Bi$_x$ (0 ≤ x ≤ 1) alloys studied by different exchange-correlation functionals, special quasi-random structures and Monte Carlo simulations.* Computational condensed matter 5 (2015), 7 – 13.

10. J. Mäkelä, M. Tuominen , **M. Yasir** , M. Kuzmin, J. Dahl, M.P.J. Punkkinen , P. Laukkanen, K. Kokko *Thermally assisted oxidation of GaSb(100) and the effect of initial oxide phases.* Applied Surface Science (2016).

1. Introduction

A junction containing a thin metal oxide film on top of a semiconductor crystal is a building block of many devices such as transistor (MOSFET, HEMT), solar cell, and several types of sensors or detectors. The efficiency of the devices has often a significant dependence on the quality of the interface between a metal oxide-film and semiconductor crystal. A detailed research of atomic and electronic structure of these interfaces is crucial in order to understand the properties of the devices. Experimental characterization of the interfaces with atomic resolution has been however hindered because the interface layers are thin and buried. One of the main challenges in the preparation of metal-oxide/semiconductor junctions has been to avoid the oxidation of a semiconductor surface during the oxide growth, which causes the degradation of interface in many cases. Another issue is to understand metal interaction with semiconductor, and finally to figure out the best approach to grow a metal-oxide/semiconductor structure with minimal harmful defects.

1.1 Metal oxide films

Metal oxides are one of the most studied material systems because they exhibit a wide range of the chemical and physical properties. They can be found as a simple binary compound when a metal cation reacts with an oxygen-containing environment (e.g., Fe_2O_3 and NiO) or in more complex forms such as [$SrTiO_3$ and $Pb(ZrTi)O_3$] if more than one metal element are involved in the formation of oxide.[1] The oxides show vast variations in the properties which depend on their metal cation(s) and crystal structure. They comprise diverse magnetic properties like antiferromagnetism (NiO) and ferromagnetism (Fe_3O_4).[2] Some oxide materials such as $BaTiO_3$ or ZnO are used for temperature sensitive resistors because they show an increase in the specific resistivity with the increase in the temperature, this property is called positive thermal coefficient of resistivity.[3] Another interesting phenomenon is the piezoelectric

property found in some metal oxides like $Pb(ZrTi)O_3$, which can be used for motion sensor devices.[4] Last but not least, metal oxides are used as a catalyst for oxidation of hydrocarbon, reduction of nitrogen oxides, and for oxidation of water (i.e. hydrogen production).[4]

Concerning their electrical properties, a metal oxide can be a superconductor (e.g., YBCO, yttrium barium copper oxide), metal (e.g., CrO_2, chromium oxide), semiconductor (e.g., $Fe_{0.9}O$, iron oxide) or insulator (e.g., BaO, barium oxide).[2,3] These variations in the conductivity have also technical importance in many areas especially for microelectronics applications. For example high k dielectric film of HfO_2 has replaced SiO_2, a step forward to reduce the size of MOSCAPs (metal oxide semiconductor capacitors).[3,4] Ferroelectric oxide like PZT (lead zirconium titantate) is used for advanced nonvolatile computer memories, where it can keep the charge stored if the power is switched off due to permanent charge polarization. Apart from this, many other technologically important functionalities like high temperature superconductivity and colossal magnetoresistance have been explored in oxide samples.[4] Most metal oxides appear in amorphous or polycrystalline form, but with careful tuning of growth parameters, monocrystalline (i.e., single crystal) oxide films have also been produced.[5-7] Single crystalline films have advantages over amorphous or polycrystalline because the crystals naturally contain fewer defects. Furthermore, crystalline materials provide a well-defined platform for fundamental studies via both experimental and computational methods. Fig 1 shows the difference between amorphous, polycrystalline and single crystalline solids.

There are several methods to synthesize the metal oxide film. First of all, most metals react strongly with oxygen and become oxidized even in a slight contact with oxygen-containing environment. It means that a metal oxide film is usually formed at surface parts of a metal piece when it is in air, for

example. Furthermore, the growth methods of metal oxides include atomic layer deposition,[8] chemical vapor deposition,[9] molecular beam epitaxy,[10] and pulsed laser deposition.[11]
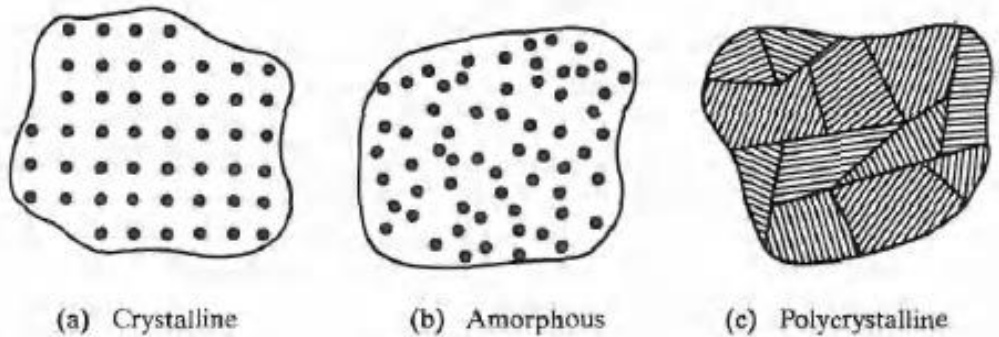

Figure 1. Three different categories of solids according to ordered arrangements of atoms in that solid. (a) Crystalline solid with more ordered structure. (b) Amorphous where the atoms are arranged randomly and not following any ordering at all. (c) Polycrystalline structure where multiple short range order exist at different orientations. The figure is taken from ref. 4.

1.2   Semiconductors

The solid materials, based on their electrical conductivity, are traditionally classified into three basic categories: conductors, semiconductors, and insulators. In a solid, atoms are close to each other, and due to the interaction of neighboring atoms, valence electron states of individual atoms are modified and split into electronic bands. The resulted electron states have energies different from discrete levels of the corresponding isolated atoms. These split electronic bands are termed as valence band and conduction band. Both bands are composed of very closely packed allowed electron energy states, but in the case of valence band these energy states are filled with electrons while in conduction band these allowed states are empty.

In the case of pure semiconductors at low temperatures, the valence bands are fully occupied by electrons, and there is a forbidden energy band gap between the valence-band maximum and the next allowed electron states in the conduction band (called conduction band minimum). In other words, there is no

electron state in the band gap of pure, defect-free semiconductor crystal. The width of this forbidden band gap determines many characteristics of the solid; e.g., whether it is an insulator, semiconductor or conductor. For conductors, the valence and conduction bands are overlapped or the band is half filled, enabling an easy excitation of electrons into empty states and thus a high electric conductivity of the metals. In contrast, for insulators the forbidden energy gap is large (typically >3 eV), and therefore the electron transition from the valence band to the conduction band over the gap is not probable by means of the thermal excitation. In semiconductors, there is a moderate energy band gap, making the thermal excitation more probable than in insulators. However, the electron density in the conduction band of a pure semiconductor crystal with the band gap higher than ~ 0.5 eV is very small as compared to metals. Fortunately, a density of electric carriers in semiconductors can be altered by means of the controlled doping and optical excitation, for example, making them suitable materials for various applications.[4,12]

Semiconductor crystals play a key role especially in the area of microelectronics and photonic devices. Two main types of semiconductors are elemental semiconductors (silicon, Si and germanium, Ge) and compound semiconductors which are formed with two or more different elements of the periodic table, for example IV-IV (SiGe), III-V (GaAs, GaInAsN), and II-VI (ZnSe). Silicon has been the main material in semiconductor industry for decades due to its electrical performance and abundance as well as top refined processing technology. Si has been used, for instance, in transistors and rectifier of integrated circuits. Also, Si is the main material of solar cells but it shows low efficiency for light-emitting applications like LED because of its indirect bandgap.[13]

The III-V compound semiconductors, with the direct band gap and higher charge velocity are used, for instance, in light detectors, LEDs, laser

diodes, and high frequency transistors. Another benefit of III-V compound semiconductors is the possibility to change the band gap by changing the composition of III-V's films in the heterostructure stacks of thin films of different band-gap semiconductors. Such band gap engineering shows clear advantages for lighting and high speed transistors technology.[14]

1.2.1 Atomic and electronic structure

Most semiconductor materials utilized in industry are in crystalline form, where the atoms have a well-defined order, as described above. The elemental semiconductors like Si and Ge contain the diamond structure where each atom is bonded to four neighboring atoms. The Bravais lattice of the diamond crystal is face centered cubic (FCC); the diamond structure consists of two overlapping FCC lattices. Many of the III-V semiconductors follow the same diamond lattice but the four neighbors of each atom are opposite type. This lattice structure is called zincblende. The valence structure of both the elemental and III-V compound semiconductors forms via localized sp^3 hybridized orbitals. While the single Si and Ge atoms possess the outer orbitals having the s^2p^2 configuration, these orbitals in the crystal become shared via the sp^3 hybridization, leading to the covalent bonding between the neighboring atoms. Likewise, in III-V semiconductors, the s^2p^1 valence orbitals of group III elements interact with s^2p^3 valence orbitals of group V atoms, via forming the sp^3 hybridized states. The formed covalent bonds, each of which contains two electrons, have a tetrahedral geometry, and thus each atom achieves the octet-rule type electron environment or distribution.[15] The compound semiconductors exhibit, in addition to covalent, also ionic character. The ionic contribution arises from the difference between the electronegativity of constituents.

Once a semiconductor crystal is truncated and a surface is formed, some of the sp^3 type bonds are broken, causing energetically unfavorable dangling bonds of the surface atoms. An example of energy levels of hybrid sp^3

dangling bond states of GaAs is shown in Fig 2. To minimize the energy, the semiconductor surface tends to reconstruct. A brief introduction to the reconstruction phenomenon is given in the chapter 1.2.2.

In semiconductors, a position of the Fermi level has an important role. The Fermi level is the energy below which all the electron states are occupied at temperature (T) = 0 K. For metals, the Fermi level simply corresponds to the highest occupied electron state when the temperature is T = 0 K, but in semiconductors, the Fermi level often lies in the forbidden band gap. Thus, the Fermi level can be defined as the energy where the Fermi-Dirac distribution gives the occupation probability of 0.5.

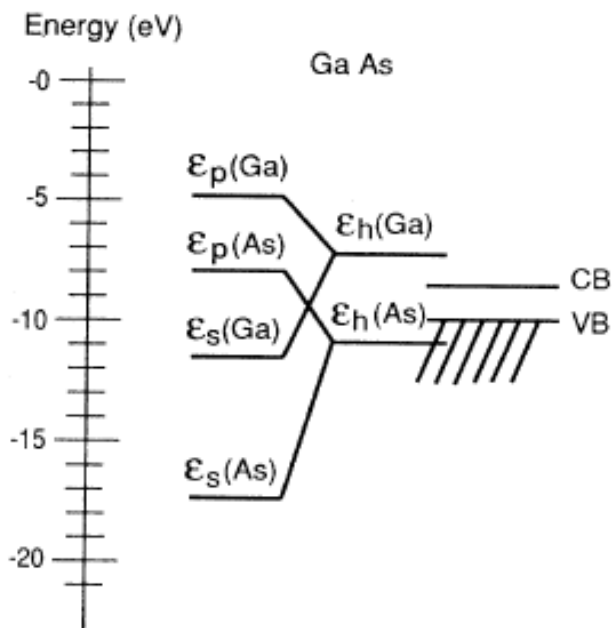**Figure 2. The Energy levels of hybrid sp3 dangling bond states of GaAs. The figure is taken from ref. 27.**

For intrinsic semiconductors, the position of Fermi level is half way between the valence-band maximum (VBM) and conduction-band minimum (CBM). A change in the Fermi level position can be induced by means of doping of semiconductor material. The doping is controlled substitution of part

of the host atoms by impurities in the crystal lattice, which significantly changes carrier concentration (holes in valence band or electrons in conduction band) and alter the electrical properties of material. For example, in group IV semiconductor materials like Si or Ge, some group V (e.g., P or Sb) or group III elements (e.g., Ga or B) are used as dopant impurities and incorporated in the crystal structure of host semiconductor material to get an 'n' or 'p' type doped semiconductor respectively. In the case of n-type doping, concentration of conductance electrons is increased due the donor impurity states near CBM, and therefore Fermi level moves close to conduction band. In contrast, in p-type materials, the valence-band hole concentration is so high that the position of Fermi level is moved close to the valence band maximum via acceptor impurity states.

1.2.2 Semiconductor surface reconstruction

Whenever a pure semiconductor surface is created, for example an ideal bulk terminated surface as shown in Fig 3(a), the dangling bonds are formed on the surface due to incomplete bonding of surface atoms, increasing the energy related to the surface structure. Therefore the surface atoms seek new bonding configurations and a surface structure rearranges in order to decrease surface energy. The structural rearrangements are usually categorized into surface relaxation and surface reconstruction. If the rearrangement happens in a way where there is no change in the surface-lattice periodicity, as compared to the bulk crystal plane, it is called surface relaxation. The relaxation involves the shifting of upper most atomic-layers in the perpendicular direction to the surface plane, and thus changes the interlayer spacing of top most layers relative to bulk crystal, as shown in Fig 3(b). If the surface atoms are displaced in a way where the surface periodicity is disturbed, then the rearranged surface is called the reconstruction, and it involves the change in the surface unit cell as shown in Fig 3(c). The semiconductor surface reconstruction can happen for atomically

cleaned crystals in vacuum or it can also be induced by adsorbate, an overlayer of another atomic species deposited on the surface of the semiconductor substrate.
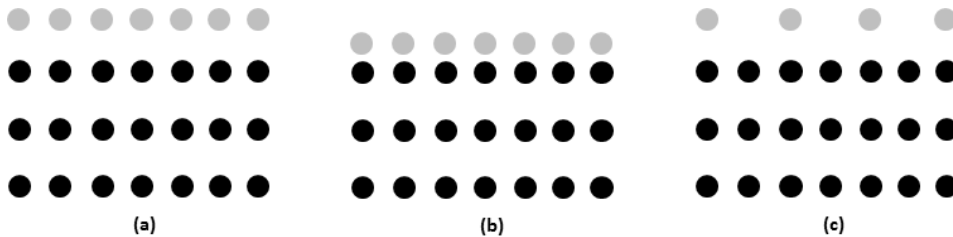

Figure 3. The Figure shows examples of (a) an ideal bulk terminated surface(b) relaxed surface(c) reconstructed surface.

There are some general principles to explain the semiconductor surface reconstructions.[16-17] On the basis of these principles it can also be predicted the surface structures appearing on the clean or adsorbate-covered semiconductor surfaces. These principles can be applied for elemental semiconductors (Si and Ge) as well as compound semiconductors (e.g, GaAs and InAs). The former contain directional covalent bonds while the latter contain partially ionic covalent bonds, but both semiconductors comprise of tetrahedral coordinated atomic geometry in the bulk.[16, 17]

Principle 1. For an unrelaxed surface, due to dangling bonds, the surface energy is lowered via rehybridization of surface bonds.

The unsaturated bonds (dangling bonds) appear, when a surface is formed, and contain unpaired electrons. To minimize the amount of the dangling bonds and to saturate (fill or empty) them, the surface atoms can form new bonds, and electronic orbitals can be rehybridized at a surface layer. For example, on Si(100) the number of the dangling bonds is halved by the dimerization (pair formation) of surface atoms as illustrated in Fig 4a.
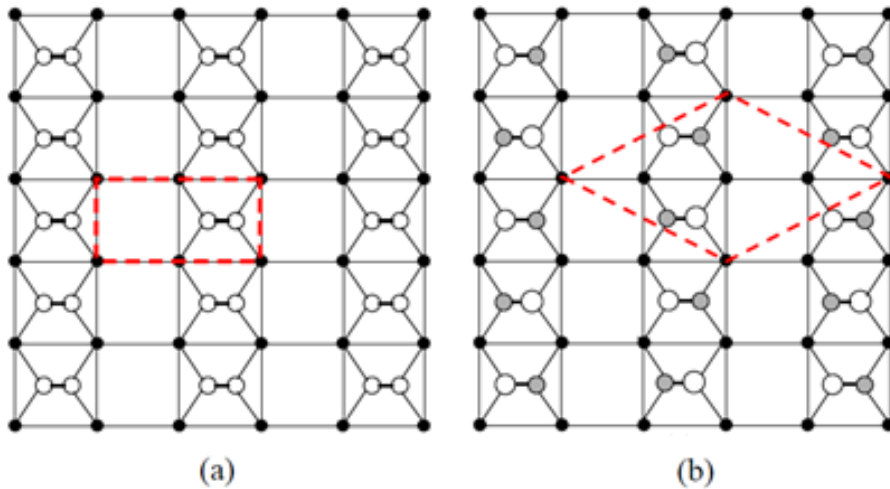
Figure 4. Top view representation of different Si (100) unit cells (a) dimiraization of surface dangling bonds (b) buckling of dimer in up and down dimer atoms in alternative rows. The figure is taken from ref. 35.

Principle 2.   A semiconductor surface tends to have a semiconducting band structure.

For example on Si(100), the tilting of the dimer axis (i.e., making the dimer buckled) shifts the electron states associated with the dimer-up and dimer-down atoms (Fig.4b) so that a band gap opens and the electron states are removed from the Fermi level. This leads to the formation of fully occupied and unoccupied dangling-bonds states. This surface band gap is approximately half of the Si bulk band gap (i.e., ≈ 0.6 eV).

Principle 3. Electrostatic (Coulombic) interaction between localized occupied orbitals tends to decrease.

This is related to the above-mentioned localization of charge in the saturated dangling bonds.

Principle 4. The surface strain tends to be minimized.

A rearranged layer of a semiconductor usually needs to follow the lattice of bulk crystal below the surface because of the strong covalent bonds. Thus, the surface part can be considered as a thin epitaxial layer on the bulk crystal.

Principle 5. The observed reconstructed surface will be the one which is kinetically favored surface for a given surface preparation condition.

In general, the above principles can compete to each other (e.g., Principles 1 and 4), and the driving force for the formation of any surface structure is ultimately a delicate balance of all these principles. In addition, there can be energy barrier(s) for the lowest energy structures, and thus surface kinetics can affect which surface structure appears in practice. For instance, at low surface preparation temperatures, a metastable structure can form instead of the lowest energy structure(s).

The above principles largely govern also the formation of the surface structures induced by the adsorbates. In addition, the chemical nature of adsorbates also plays a role; for example, it is energetically favored for many semiconductor elements to form a bond with oxygen instead of many other elements.

1.3 The oxide/semiconductor junctions

The synthesis of an oxide film over semiconductor substrate creates an oxide-semiconductor junction (OSJ). The formation of a thin interface layer at OSJ, during the growth of oxide film on semiconductor crystal, affects the performance of many applications such as transistors[18], solar cells[19,20], touchscreen technology,[21] and water splitting photoelectrochemical cells.[22] Below it is introduced only one example: transistor in more detail.
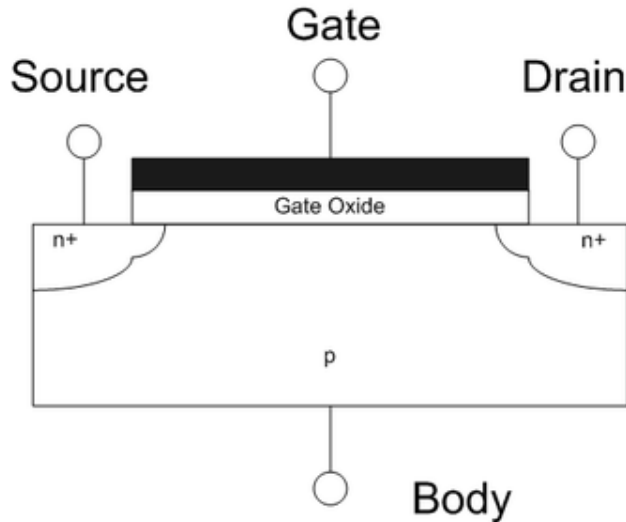
A few nanometers thick oxide layer is the key player of device performance in metal oxide semiconductor field effect transistors (MOSFET) which are the heart of electronics. A MOSFET is a 3- electrode device and these electrodes are called source, gate and drain as it is shown in Fig 5. The gate terminal is separated from the body by a thin insulating film of gate oxide below which the conducting channel is formed. The conductivity of the semiconductor channel is controlled by applying an electric field on gate terminal which modulates the charge separation in the gate-dielectric region so that the electric charges can flow between source and drain. The importance of interface quality of OSJ is undeniable for revolutionary microelectronics industry; the credit goes to the silicon dioxide (SiO_2) which is a naturally stable oxide to be used as efficient gate dielectric film on silicon (Si) substrates. The great benefit of SiO_2/Si is that its interface defects can be passivated by hydrogen, allowing enough high performance for MOSFET. Due to the aggressive size scaling of transistors for improved functionality within the certain dimensions, SiO_2 has been replaced with HfO_2 in high performance microprocessors.[15] HfO_2 is called the high permittivity (or high dielectric

constant 'k') oxide; its $k{\sim}27$ is high compared to that of SiO_2 ($k = 3.9$). The Fig.6 shows an increase in the capacitance and a decrease in the gate leakage current when the SiO_2 is replaced with a high-k gate dielectric film. Since the capacitance of a MOS capacitor increases with decrease in dielectric thickness and with increase of the k value, therefore the use of high-k films allows the thicker oxide layer to minimize the harmful leakage current through the oxide film, as compared to the SiO_2 junctions. Yet, HfO_2/Si interface contains a thin SiO_x layer because the Si oxidation is energetically so favored process.

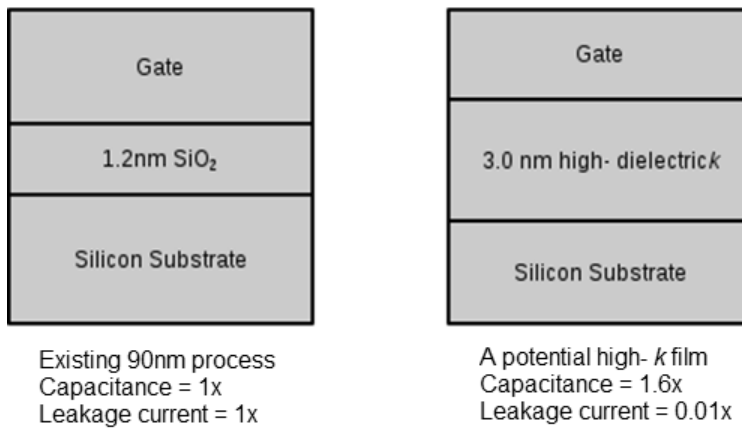|	
Gate	Gate
1.2nm SiO_2	3.0 nm high- dielectric$k$
Silicon Substrate	Silicon Substrate
Existing 90nm process Capacitance = 1x Leakage current = 1x	A potential high-k film Capacitance = 1.6x Leakage current = 0.01x

Figure 6. A comparison of SiO_2 with high–k dielectric as gate insulating film over Silicon substrate showing the difference of deposited film thickness and corresponding leakage current and Capacitance. The figure is taken from ref. 28.

The situation is still challenging to get a device grade oxide/III-V interface due to exothermic nature of III-V surface oxidation during the MOSFET process. This oxidation results in the growth of amorphous oxide film with a high density of defect states at the OSJ interface, increasing the electron-state densities in the bandgap. The consequence of these interface states is the pinning of Fermi level position at a fixed energy point. Thus, the position of the Fermi level cannot be properly changed around the band gap by means of the gate voltage. This modulation of Fermi level as a function of gate voltage is the main characteristic of MOSFET operation and due to pinning of Fermi level, the device functionality is degraded.

This oxide related defects are very difficult to avoid during the process of oxide growth on semiconductor surface or passivation of semiconductor surface components. Synthesis of crystalline oxide structure on semiconductor surface is one of the most potential methods that can help to minimize the surface defect states formation, because the crystalline material contains naturally less defects compared to amorphous.[23-28]

1.3.1 Challenges in preparation and characterization of interface structure

An interface region is formed at the junction point of two materials when both materials are brought into contact with each other, for example; the growth of a metal-oxide film on top of semiconductor substrate. As remarked above, an oxide/semiconductor interface has a considerable technological importance for semiconductor MOSFET devices. As a rule, semiconductor materials are lacking in good quality interface because the oxidation of semiconductor is a very favorable process, and during the interface growth this uncontrolled chemical reaction can cause harmful defects states in the interface region. Avoiding this uncontrolled oxidation and engineering the interface defects have proven to be very challenging.

Once an interface is formed, probing this region is not that straightforward because it is a thin buried structure and hidden below the grown film which can usually be much thicker than the interface region. Transmission electron microscopy (TEM) is one rare tool to characterize a local structure of the buried interface with atomic scale resolution. Photoelectron spectroscopy (PES) is also a potential technique to determine the local atomic environment and bonding configuration at interface layer, because the elastic electron signal can be obtained from buried interfaces through the topmost film. Moreover, PES is a nondestructive tool. In this work this method has been widely utilized.

2. Experiments

2.1 Surface preparation

An atomically clean and ordered semiconductor surface free of impurities and native oxides provides an ideal platform for the junction preparation when a thin film is deposited upon such a surface. The initial surface structure of the substrate often has an essential influence (in addition to the growth temperature) on the formation of growing film and film/substrate interface. Several methods are adopted to achieve a clean semiconductor surface including ion-sputtering[29], heating with high current pulses[30] and chemical treatments like; ammonia treatment[31], HCl-isopropanol treatment[32], halogenation[33] and etc. Not every method can be applied to all semiconductors. For example the flashing method where high current pulses are applied across the sample is useful to remove most of the impurities from Si sample because the temperature required removing surface oxides and carbides are below the melting point of Si. In contrast, III-V semiconductors start to melt before surface oxides and other contaminants desorb from the surface.

Ion sputtering is another extensively used method in surface-science laboratories where high energy ions of inert gases (usually argon gas) are bombarded on the sample surface followed by the annealing cycles to clean it from unwanted oxide layers. The annealing temperature can be selected according to semiconductor material one is dealing with, for instance, GaAs substrate can be stable up to 600 ^{O}C but some other III-V materials like InAs or InSb cannot sustain at this temperature because of their low melting points. The purpose of the post heating is to recover a crystal structure, which is destroyed at surfaces due to the bombardment. In this work, we used both the Ar-ion sputtering method (for III-V's and Ge) and also the direct-current flashing (for Si). In the latter, we quickly applied high current for short period of time to the

Si substrate to heat the sample close to 1200 $^{\circ}$C . We repeat this current pulsating method few times so that all the contaminations are removed from the sample surface.

2.2   Thin film synthesis and film oxidation

As discussed in the first chapter, there are several approaches to grow metal-oxide films. To synthesize these metal oxides films on semiconductor substrate, we used two methods: physical vapor deposition (PVD) method or chemical vapor deposition (CVD) method. We used the PVD method to deposit (or evaporate) metals in our experiments. In this method, the metal is heated with an electrical resistive heating method in UHV conditions. At a high temperature metal is vaporized and a metal cloud is formed inside the chamber. These vapors are then transported to the substrate and impinge on the sample surface and finally the surface is coated with film of that metal as shown in the Fig 7. This method is called thermal evaporation method.
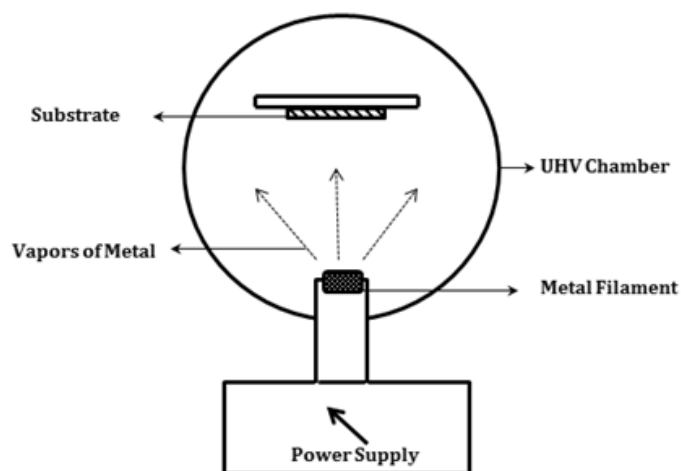

Figure 7. Schematic top view representation of resistive thermal evaporation method

The film oxidation is performed by introducing oxygen in the chamber either during thermal evaporation of metals or after the growth of metallic film on sample.

Atomic layer deposition (ALD) is a vapor phase thin film deposition method used for the film fabrication in industrial and research laboratories. A hand-made small scale ALD system is installed in our laboratory for the Al_2O_3 film deposition. This method provides a film conformality and control of film thickness and composition.[33] In this technique, the surface of the substrate is exposed by precursors of required film (for example Al and O containing gases). It is a process where gaseous precursors are sent to the substrate in separate pulses in a sequential manner as shown in Fig 8.
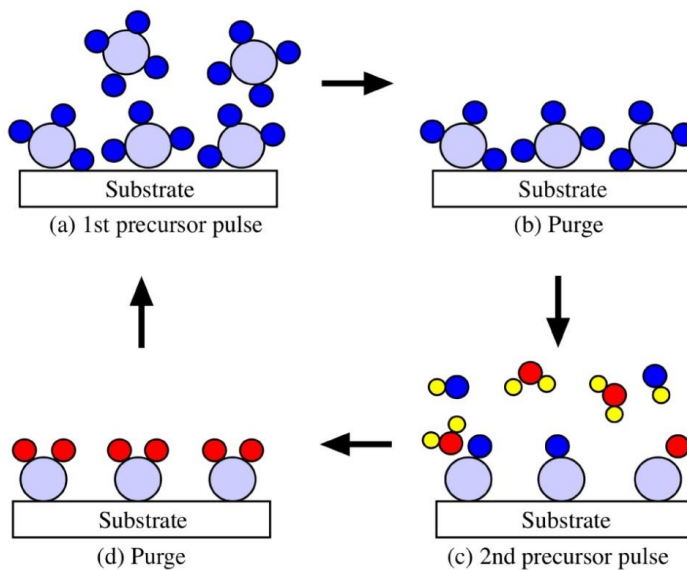

Figure 8. Schematic representation of the basic steps involved in ALD process. The figure is taken from ref. 35

In the first pulse, the precursor has enough time to fully react with the surface of sample, then the system is purged by introducing an inert gas into the chamber to remove the unreacted precursors after this the pulse of second precursor is sent that reacts with the surface and then once again the purging of the chamber is performed by using inert gas to remove the byproducts of the reaction. The cycles of alternating pulses continue to perform layer by layer growth of desired film until the required film thickness is achieved.

3. Characterization methods

The properties of a clean and well-defined surface are necessary to study in well-justified manner. To preserve a clean surface for some time, an ultrahigh vacuum (UHV) condition ($\sim 10^{-10}$ mbar) is necessary. To get insight into the surface and interface properties, a single characterization technique is not enough, as usual, and therefore a combination of complementary surface sensitive techniques should be used to properly characterize the surface.

The surface science instrument that we have used in the laboratory of University of Turku, consists of low energy electron diffraction (LEED), scanning tunneling microscopy (STM) and x-ray photoelectron spectroscopy (XPS) methods combined in the same UHV system. The high-resolution electron spectroscopy has been also applied at the MaxLab, an international synchrotron-radiation center located in Lund, Sweden. The photoluminescence (PL) and capacitance-voltage (CV) measurements were made via the collaboration with Tampere University of Technology and Department of Information technology, University of Turku.

3.1 Low energy electron diffraction (LEED)

LEED is the common method to study the periodicity of the surface atomic structure. A LEED instrument consists of an electron gun, a fluorescent screen to observe diffraction patterns, and a set of grids with retarding potential difference to suppress the unwanted inelastic electrons and allow only the elastically backscattered electron to pass to the screen.

When we consider only a two dimensional crystal in real space, the lattice-point distance in the surface normal direction is infinite and the diffraction will occur if the two- dimensional Laue conditions are satisfied. According to Laue, constructed interference will happen only when the resultant vector '$k_{||}$' of parallel components of wave vectors of incident beam 'k_o' and

scattered beam 'k'' is equal to a lattice vector 'g_{hk}' in reciprocal space. Mathematically this relation can be described as follows

$$\overline{k}_{||} = \overline{g}_{hk} \tag{1}$$

$$\overline{k}_{||} = (\overline{k}'_{||} - \overline{k}_{||o}) \tag{2}$$

Geometrically, it can be represented with the construction of Ewald sphere in 2D as shown in Fig. 9. Since the real-space periodicity perpendicular to surface is infinite, the points in the reciprocal space, due to inverse relation between real and reciprocal space, will be infinitely dense and forming rods.
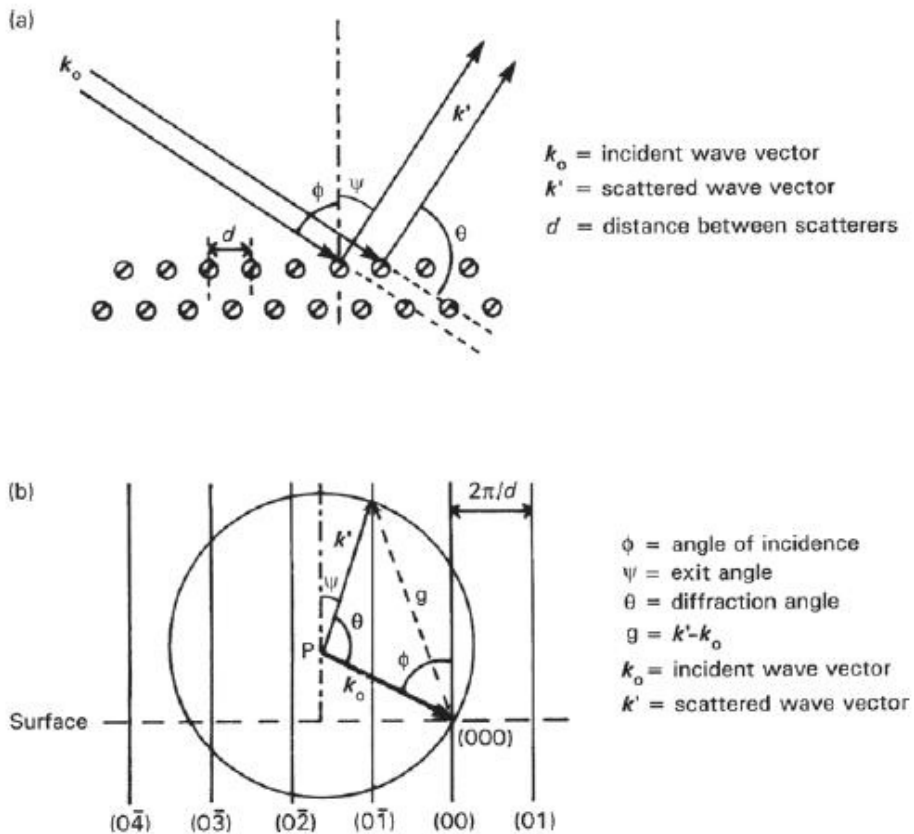

Figure 9. A Schematic illustration of (a) diffraction process occurring at the 2D plane. (b) Construction of Ewald sphere in reciprocal space. The figure is taken from ref. 37.

The diffraction condition is satisfied only when these reciprocal rods intersect the Ewald sphere and each intersection point is a represented by the reciprocal-space coordinates (hk). The radius of the sphere can be changed with the change in the energy of incident electron beam.

A representation of schematic experimental setup is shown in Fig.10. The electrons are generated in the electron gun filament and then accelerated with a voltage of 20V- 200V which correspond to wavelength $\lambda_E = 0.87 - 2.75$Å using the de-Broglie hypothesis where a beam of electrons can be considered as (free electrons) plane wave via a relation,

$$\lambda = \frac{h}{p} = \frac{h}{\sqrt{2meV}} \tag{3}$$

Where 'h' is Plank's constant and 'm' and 'e' are the rest mass and charge of electron, respectively, and V is the applied voltage to accelerate the electrons. When the incident electron beam is perpendicular to the surface plane, the diffraction condition can be described also with the Bragg law:

$$d \cdot sin\Psi = n\lambda. \tag{4}$$

The probed elastic electrons with this energy range show a minimum in the universal mean-free path curve; so the technique is surface sensitive. The wavelength is of the order of interatomic spacing, and therefore electrons are backscattered by the surface planes when they are bombarded to the sample surface in the surface normal direction. A diffraction pattern is formed by these backscattered electrons on the screen, which is actually a map or picture of the reciprocal-space lattice, as visualized in the real space. This information is routinely checked to determine the surface symmetry and also the shape and size of surface unit cell. The intensity of the spots is sharp and bright in the LEED pattern if the surface acquires a well-crystalline structure.
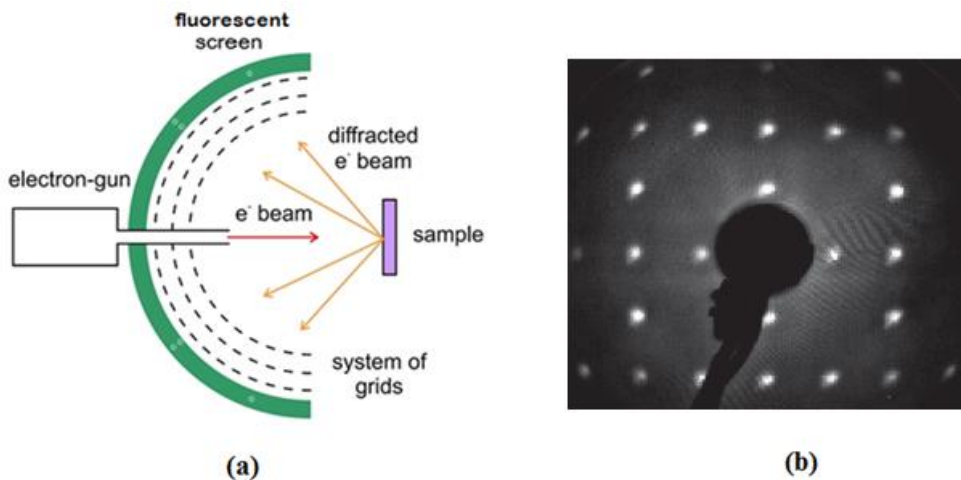
Figure 10. (a) A schematic representation of experimental setup of LEED. (b) Si(100)(1×2) - Sr. The figure(a) is taken from ref. 38.

3.2   Photoelectron spectroscopy (PES)

Photoelectron spectroscopy (PES) is perhaps the most used surface characterization method. When a material surface is illuminated with photons, they knock out the photoelectrons from material to the vacuum with a kinetic energy E_k depending on the photon energy, the work function of that material and amount of inelastic scattering. These photoelectrons are then collected by a detector or electron energy analyzer. For elastic electrons, the kinetic energy of an emitted electron can be described by using the equation

$$E_k = h\upsilon - \varphi - E_B \qquad (5)$$

Here E_k is the photoelectron kinetic energy, φ is the work function of analyzer, E_B is the binding energy of electrons and $h\upsilon$ is the energy of illuminated photons. On the basis of the kinetic energy of detected electrons, the information about the chemical composition of a sample and the electronic state of atoms present in the sample can be deduced. PES can be categorized into three methods:[40] ultraviolet photoelectron (UPS), soft x-ray photoelectron spectroscopy (SXPS) and x-ray photoelectron spectroscopy (XPS), depending on the energy range of the incident photons. In UPS the photon energies range

from 5 to 50 eV and it can be performed using a helium discharge lamp. Due to this low energy range, the method is useful to study the valence-band structure of the material. In SXPS and XPS the photon energy ranges are 50-1000 eV and 1000-1486.7 eV, respectively.[41] The fourth category of PES, which is called hard x-ray photoelectron spectroscopy (HAXPES), covers the energies above than 1486.7 eV. At home laboratories, magnesium (Mg) and aluminum (Al) anodes are utilized as x-ray sources that emit the photons with the emission energies of ~1486.6 eV for Al K_α and ~1253.6 eV for Mg K_α. These energy values are sufficiently high for core level spectroscopy of wide range of elements. The photoelectron emission is best described with a simple three step model. At first step, the electrons at their initial state get excited by absorbing the incoming photons of energy $h\upsilon$ and make a transition to the final free-electron like state within the material. In the next step, electrons move towards material surface and can lose their energy in several ways. For example: via scattering with phonons and/or knocking out the electrons from valence band. Therefore the electrons which are originated deep inside the material have less chance to reach the surface. Finally, the electrons overcome the surface potential barrier and escape through the surface to the vacuum.

XPS is considered as a highly surface sensitive characterization method. The penetration depth of x-rays in the solid material is ~1 μm with a covering area around ~ 1×1 mm^2.[42] However, the photoelectron generated deep inside the material experiences inelastic collision and hence it does not to contribute in the elastic signal, which is usually the most interesting. In other words, the elastic signal mainly consist of photoelectrons coming from top most surface layers (< 10 nm) and the rest of electrons either suffer an energy loss and contribute in the background signals or trapped again in the material. This makes XPS a very surface sensitive tool. The probability $P(d)$ of an electron escape from the solid surface after travelling a distance 'd' without experiencing any inelastic scattering can be estimated by[37]

$$P(d) = e^{\frac{-d}{\lambda}} \tag{6}$$

Here d is the distance travelled by photoelectron, λ is an inelastic mean free path (IMFP) which is the average distance covered by an electron before it experiences any energy loss. The IMFP is largely independent of material but has dependence on kinetic energy of photoelectron. The above given equation tells that 95% photoelectrons that participate in the spectral peak consist of electrons generated within the sample depth of 3λ.
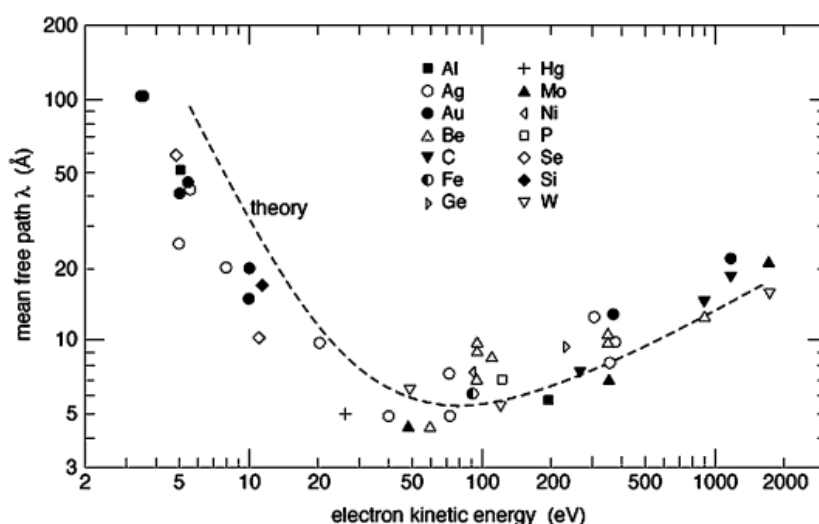

Figure 11. Inelastic mean free path for electrons as a function of kinetic energy. The figure is taken from ref. 43.

A plot of IMFP as a function of kinetic energy of electron is shown in Fig 11. The plot shows a minimum for the kinetic energy of photoelectron values ranges 50-100 eV which indicates the surface sensitivity of these photoelectrons.

Every element has a set of unique binding energies for corresponding s, p, d or f orbitals and taken this property into account, the elements present in a material can be identified via an XPS spectrum. In addition to this, a high resolution XPS spectrum can also be used to identify the different chemical or

bonding environment of the same element. For example, in the simple initial state model, where we do not consider the screening effect, the surface atoms have a valence electron charge state different from that of bulk atoms due to different bonding environment, and therefore the core-level binding energy of surface atoms is not the same as that of bulk atoms. The difference of such states usually leads to additional components shifted relative to the bulk one, making the spectral line shape more complicated, as can be seen in the Fig 12 for the Si(100)(2x1)+(1x2) surface. A high resolution spectrum is needed to resolve minor changes in the binding energy and to deduce change(s) in the bonding environment. For example in Fig. 12, the emission components (so called surface core level shifts) for the different Si surface atoms (Fig. 4) are represented by S_u, S_d, S_1 and S_2 separated by the Si 2p bulk B peak. The upper atom of asymmetric dimers of Si surface shows a clear shift (a component S_u at about 0.5 eV) to low binding energy compared to the bulk component and the down atom S_d. The reason behind the shifting of the S_u atoms towards lower binding energy is that in the buckled dimer, the valence charge is partly transferred from the dimer-down atom to the dimer-up atom. The presence of additional valence electron charge on the dimer-up atom results in that this atom has a core-level binding energy lower than that of the bulk and dimer-down atoms. While the S_1 and S_2 components are resulted from reconstructed sub layers and Si atoms present in the second layer, respectively. [44-45] Though the origin of extended components is not very clear, it is considered that these peaks correspond to some surface structure related defects.[44] The synchrotron sources are the suitable equipment to resolve these minor shifts in the binding energy, because of very high resolution with high photon intensity and tunable photon energies to a wide range.

In the measured XPS spectrum, the spectral lines become broadened. This broadening is connected with some physical and instrumental reasons. The physical factors involves the quantum mechanical state of material where the

life time 'τ' of resultant core hole, after emission of photoelectron, has some uncertainty. This imposes the uncertainty in energy of core hole state due to the Heisenberg's uncertainty principle which results as natural width 'Γ' of the energy state.

$$\Gamma = \frac{\hbar}{\tau} \tag{7}$$

Where $\hbar$ is the Planck constant, τ is the life time of core-hole state and Γ is the natural peak width. The deeper core level state, the shorter the life time of core hole and larger will be the peak width. Therefore the natural peak width of a 4s level will be higher than the peak width of 4p level in the homogeneous material of same element. This natural broadening is described by the Lorentzian peak profile when the spectral fitting is performed. The Gaussian profile is used to describe the instrumental broadening, thermal broadening and also the local disorder. The instrumental broadening may arise due to the photon bandwidth because they are not ideally monochromatic and also effect with the resolution of photoelectron detector.
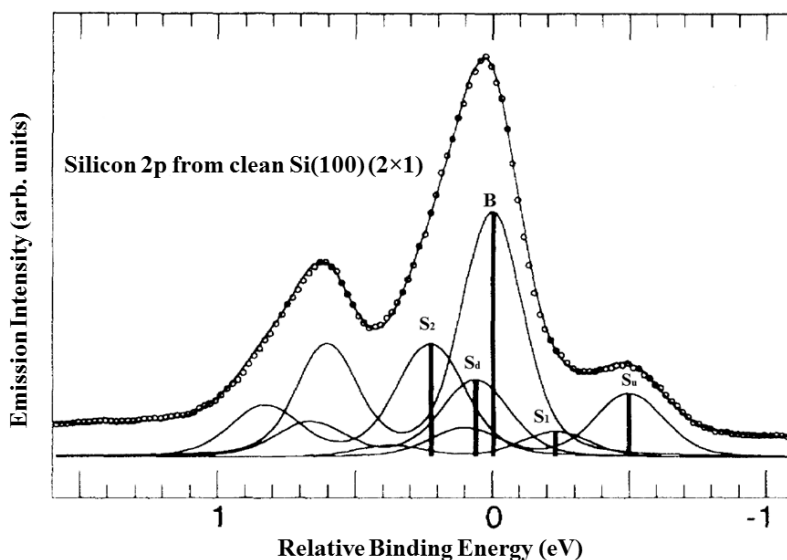

Figure 12. A high resolution Silicon 2p spectrum that shows the different resolve components form surface. The figure is taken from ref. 59.

In XPS, a vast variation is observed in the sensitivity factors of different elements. A trend shows that the lighter elements are less sensitive than heavier elements because with heavier elements the probability of photoionization is also increased. In a case of LiF where the material contains equal amount of both Li and F atoms, but there is a significant difference in the peak areas of Li 1s and F 1s because F has sensitivity ~ 1 which is 40 time higher than the sensitivity of Li ~ 0.025.[46]

3.2.1 Spectral fitting

The two main features of a core-level spectrum are peak intensity and peak position, the former deals with the amount of one element present in the specimen while the latter one gives the information about the bonding environment of element. In order to analyze a core-level spectrum, the spectral fitting procedure is performed to resolve the different components contributing in the peak area. The fitting procedure used in this work mainly involves the setting up of reasoned input parameters: the subtraction of background signals, dealing with peak width broadening, the splitting of spin-orbit doublet and the branching ratio. Since the probability of electrons to leave the specimen without experiencing the inelastic scattering is very low for electrons reside deeper than 3λ (see (6)), therefore these electrons do not contribute in the main peak but generate the background signal. The removal of this background signal can be performed using the Shirley's method.[47] Voigt profile, which is the convolution of the Lorentzian and the Gaussian distribution function, is used to account for the peak width broadening in the case of semiconductors and dielectrics. The spin orbit splitting occurs when the electron's spin and orbital angular momentum interact with each other and break the peak into components separated with certain energy value.[40] Branching ratio is used to obtain the intensity ratio of components split via spin-orbit interaction. The intensity ratio is evaluated by orbital quantum number l and it should be close to the statistical

value of $(l+1)/l$. *For* example; the As $3d$ doublet peak (As $3d_{5/2}$ and As $3d_{3/2}$) having an orbital quantum number '2' (for d-orbital) therefore acquire the intensity ratio of 3:2 with a peak separation of ~ 0.69 eV between the As $3d_{5/2}$ and As $3d_{3/2}$ peaks. An example of fitted spectrum for As 3d peak, from GaAs sample, is given in the Fig. 13, where the core-level components (shifts) due to different bonding environment of As (As-As, As_xO_y and As_2O_3). Each component consists of two peaks: As $3d_{5/2}$ and As $3d_{3/2}$.
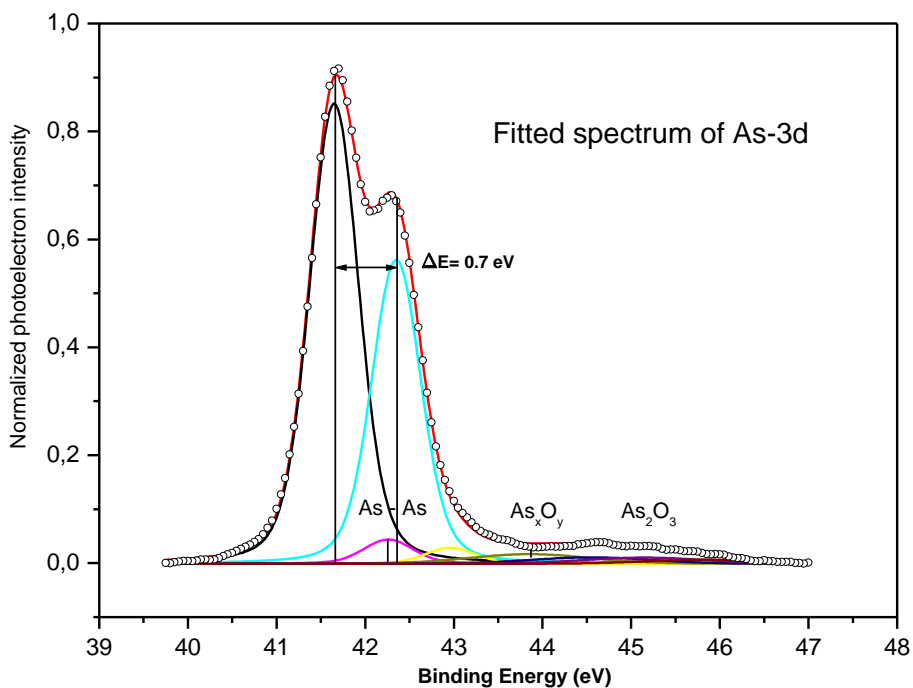

Figure 13. Fitted Spectrum of As 3d peak from GaAs sample. A spin- orbit doublet of As-3d (i.e, As $3d_{5/2}$ and As $3d_{3/2}$) with the peak separation of 0.7 eV can also be seen in this figure.

3.2.2 Synchrotron radiation based photoelectron spectroscopy

There are several advantages of using a synchrotron source for XPS measurement as compared to traditional home laboratory x-ray source. It includes high luminosity, wide range of tunable photon energy and very high instrumental resolution which is not possible using conventional x-ray sources.

Synchrotron radiation is the result of deceleration of electrons when they follow a curve trajectory in the storage ring while moving with the relativistic velocity. The main components of modern synchrotron sources include an electron source, a linear accelerator (LINAC), different magnetic lenses (wigglers or undulators) to bend the trajectory of moving electrons, radio frequency cavity (RF- cavity) and storage ring. An schematic representation of synchrotron radiation facility is shown in Fig 14.
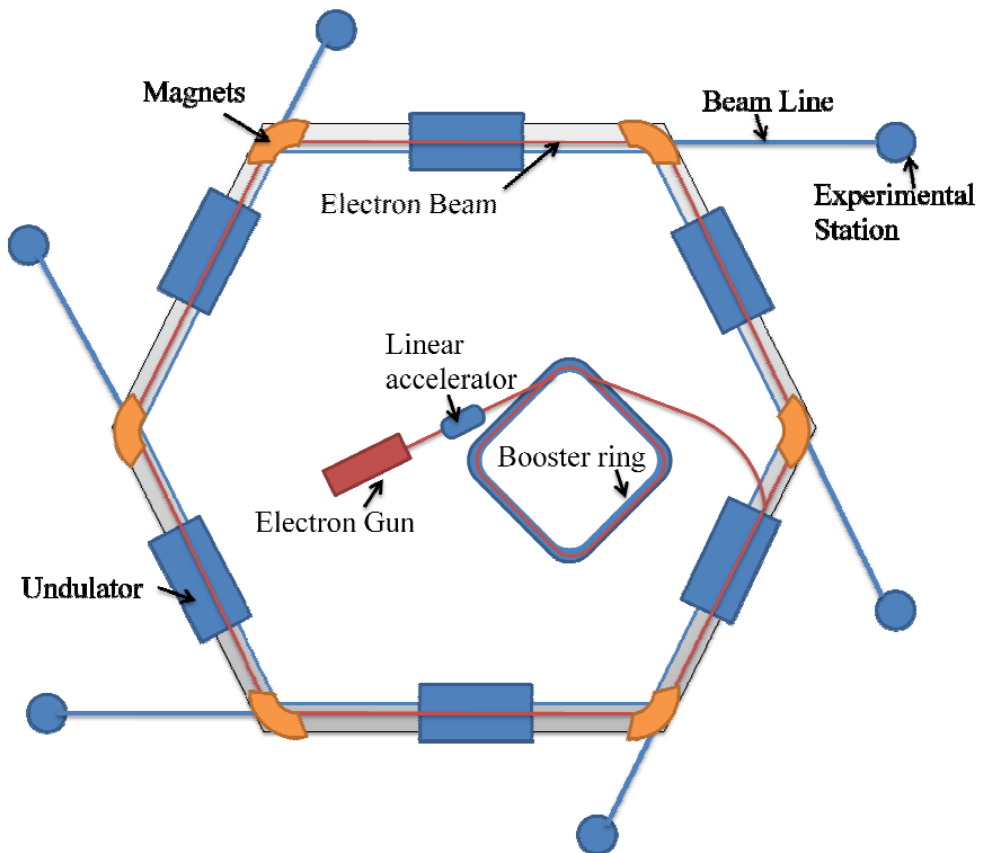

Figure 14. Schematic diagram of synchrotron radiation facility. The figure is taken from ref. 42.

Electrons, generated by heating the cathode filament, are moved to linear particle accelerator (LINAC) which transfers these electrons to the booster ring where the electron beam is accelerated by means of radio frequency waves until

they start moving close to relativistic speed and acquire the 99% speed of light, at this stage, the electron beam is injected into the storage ring. The storage ring is a closed loop where synchrotron light is generated and it is composed of series of straight and curve sections. The straight section contains undulators or wigglers, which are arrays of magnets with opposite polarity therefore when the electrons are pass through these magnetic structures they follow a wavy trajectory and produce very bright beam of radiation. The difference between wigglers and undulators is basically the magnetic field intensity and also the spacing between magnets. Undulators are operated with weak magnetic field while wigglers have comparatively high magnetic field. In the curve section, the bending magnets constrain the moving electrons to follow the curve trajectory and deviate from the straight path therefore electrons lose their energy with the emission of synchrotron radiations. These radiations are passed through a monochromator to select the radiation of specific wavelength and then used by the end station of the beamline.[42] One of the commonly used methods using synchrotron based XPS method is angle resolved photoemission spectroscopy (ARPES) which is shortly discussed in the next heading.

3.2.3. Angle resolved photoemission spectroscopy (ARPES)

The directions of the photoelectrons are also utilized especially to extract the information about surface electronic structure. In this method, the photoemission signal is detected as a function of the photoelectron emission angle. The wave vector of emitted electrons k can be decomposed into parallel and perpendicular components.

$$\overline{k} = \overline{k}_{\perp} + \overline{k}_{\parallel} \tag{8}$$

Using the Fig 15, the parallel component can be written as

$$k_{\parallel} = |k|\, sin\theta \tag{9}$$

using the kinetic energy equation for free electrons

$$k_{\parallel} = \frac{\sqrt{2m_e E_k}}{\hbar} \, sin\theta \qquad\qquad (10)$$
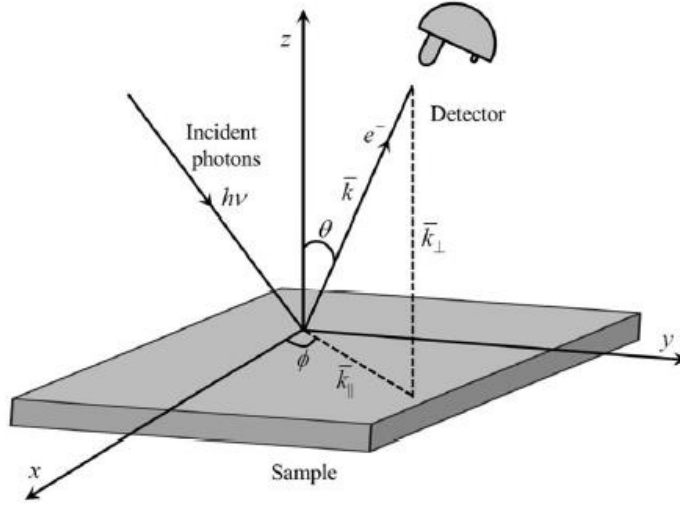

Figure 15. Geometry of an ARPES setup. The figure is taken from ref. 41.

In the photoemission process, the total energy and the momentum component parallel to the sample surface is conserved but the perpendicular component of k which is in the surface normal direction is not conserved. In this direction the translational symmetry is broken and emitted photoelectron experience a potential impact due to the work function of material while making a transition to vacuum. These measurements are very useful to probe the energy bands (i.e. E-k dispersion curves).

3.3 Scanning tunneling microscopy/spectroscopy (STM/STS)

Scanning tunneling microscopy (STM) is considered as a very exciting tool in the area of surface sciences for its ability of nanoscale surface imaging or more precisely imaging of localized electronic states. It works on the principle of quantum mechanical tunneling, which allows an electron with energy E tunnel through the vacuum barrier φ ($E<\varphi$) between the tip and the conducting surface. The main advantage of STM is the possibility to investigate real space

surface structure on the atomic scale as well as local features like steps or defects.

In STM, a very sharp metal tip (usually tungsten tip), or ideally single atom at the tip, is brought close enough to a conducting surface so that the wave function of surface and the wave function of the tip overlap to each other. A tunneling current I is introduced when a sufficient small biased voltage V between tip and sample surface is applied. This tunneling current is very sensitive to the distance between sample and the tip and it decreases exponentially if the distance is increased. There are two operating modes of surface scanning; constant current and constant distance modes. The most commonly used method is constant current mode. In this mode, the tip moves over the sample surface and changes the x and y directions by using the piezoelectric devices. The feedback electronics constantly signals the piezoelectric driver to adjust the z- direction between tip and sample so that the tunneling current can be kept constant. The height differences, during scanning, are utilized to obtain a contrast change in the STM image and represent the local electronic states or the topography of sample surface.[48] The adjustment of positive or negative biased voltage defines the selection of empty states or filled states imaging and also the direction of flow of tunneling current. For example, when a sample has positive voltage, electrons tunnel from occupied states of the tip to unoccupied states of the sample and therefore it is considered as empty states imaging.[48,49] The careful adjustment of tunneling current, speed of scanning and the feedback loop is needed to find a good topographical image. A scheme of constant-current STM operation is shown in Fig 16(a).
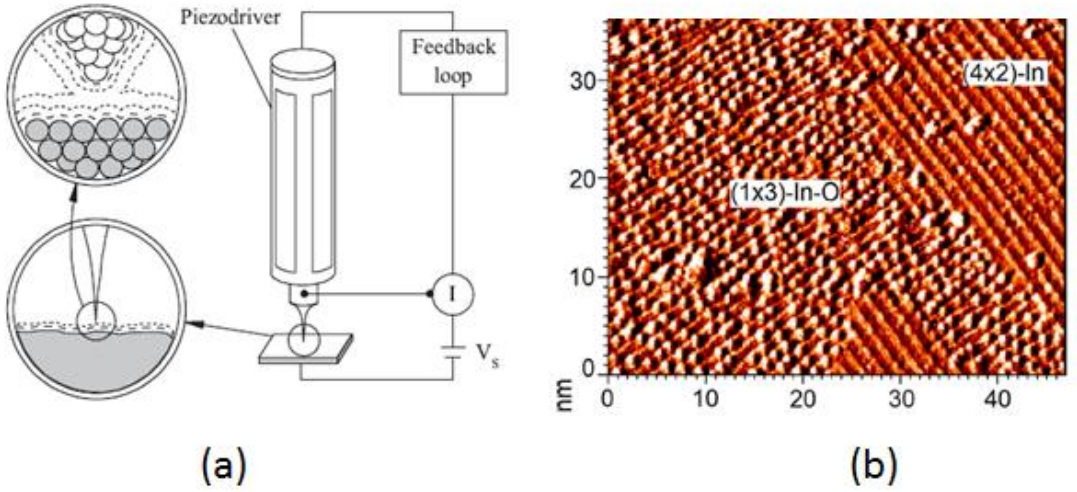
Figure 16. Schematic illustration of STM operation (a). An STM image of Indium deposited GaSb substrate. The figures are taken from ref. 50 and 51, respectively.

The STM is utilized for atomic scale imaging and it is very sensitive to the small vibrations and noise from the surroundings therefore it requires the STM instrument to be isolated from these vibrations. For this reason, STM base plate is suspended using permanent magnets that surround it. The tip geometry also has great impact on the image quality and it should be very sharp to obtain high resolution images.

Bardeen's formalism[52] shows that the tunneling current can be expressed using a first order time dependent perturbation theory

$$I = \frac{2\pi e}{\hbar} \sum_{\mu,\nu} \left\{ f(E_\mu)[1 - f(E_\nu + eV)]|M_{\mu\nu}|^2 \delta(E_\mu - E_\nu) \right\} \tag{41}$$

where E_μ and E_ν are the energies of the states $\psi_{\mu\nu}$ of sample and tip respectively, $f(E)$ is the Fermi distribution function and V is the applied biased voltage between tip and sample and $M_{\mu\nu}$ is the tunneling matrix element between the tip states and sample surface states.

The equation is approximated by Tersoff and Hamann[53] which assumed the geometry of the tip as point probe and can be described as s-wave character.

Small biased voltage and low temperature is also assumed. The equation gets the form

$$I \propto V . n_t(E_F) . e^{2\chi R} . \sum_v |\psi_v(r_o)|^2 \delta(E_v - E_F) \qquad (52)$$

where $n_t(E_F)$ is the local density of states at Fermi level of tip, $\chi = \frac{2m\phi}{h}$ depends on work function ϕ, R is the radius of the spherical tip. The local density of electronic states (LDOS) at Fermi level of point probe defines the tunneling current which has proportional relation with LDOS and since the LDOS decay exponentially if the spacing between the tip and sample increases therefore an exponential decay of tunneling current also happens with this change in distance.

In addition to the surface geometry, the STM tool can also be utilized to record spectroscopic measurement which is known as scanning tunneling spectroscopy (STS). STS is a complementary technique to STM and provides the information about the local electronic structure of the sample surface above and below the Fermi energy.
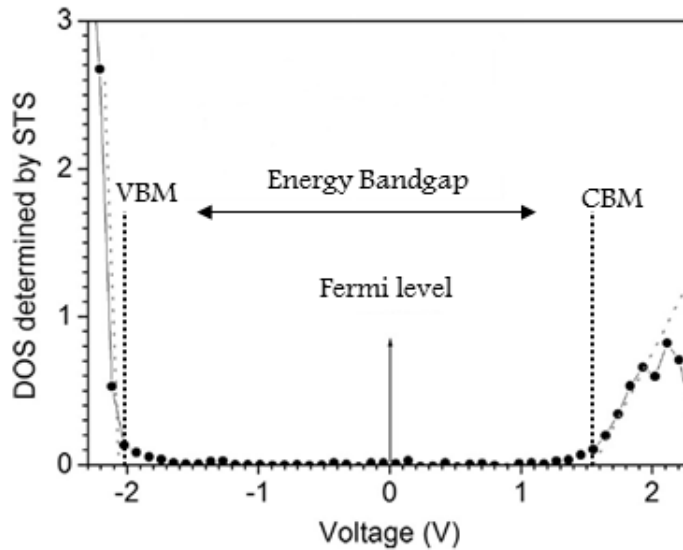

Figure 17. Scanning tunneling spectroscopy curve of Sb_2O_3 film deposited on top of Si(100) sample.

In STS, the distance between tip and sample and also the tip position is kept fixed and the feedback loop is switched off. In this work, the IV-spectra, at different position, are recorded by measuring the tunneling current as a function of sweeping biased voltage. Numerical analysis of the data provides a differential signal (dI/dV-V) which gives good approximation of LDOS of the sample. An example STS spectrum of Sb_2O_3 film is shown in Fig 17 where the band gap of the film is deduced by performing linear extrapolation at valence and conduction band edges to the voltage scale.

3.4 Photoluminescence (PL)

Photoluminescence (PL) is valuable non-destructive technique to study both the bulk and surface interface properties of semiconductors. PL is a widely used measurement in semiconductor physics and optoelectronics. The PL measurements do not require any ultrahigh vacuum environment or sample preparation before the measurements that makes it an attractive tool for usual atmospheric pressure analysis. The PL can be best described as a three step process.

step 1: An optical excitation generates electron-hole pairs when photon of sufficient energy is absorbed (energy of the photons is often clearly larger than the energy band gap).

step 2: Created electrons and holes are quickly (~ 10^{-12}s) relaxed or thermalized and occupy the energy states at conduction band minimum (CBM) or valence band maximum (VBM), respectively where they stay for relatively long time (~ 10^{-9} - 10^{-6} s) before recombination.[54] This means that electrons and holes can diffuse at CBM and VBM, respectively, hundreds of nanometers (nm) or even up to micrometer (μm) depending on the material, in a high-quality semiconductor crystal.

step 3: After the diffusion, the electrons and holes are returned to ground state and recombine in radiative or non-radiative way. The radiative spectrum is measured.

Since the excitation source is photons, the method is called photoluminescence. The resultant photons are collected to photodetectors and information can be extracted about the electronic structure around the band gap of a material. Obviously, PL is more suitable for the direct band gap materials than for indirect ones because indirect bandgap materials possess a shift between CBM and VBM in the momentum space. Therefore an additional excitation or relaxation of momentum require for radiative recombination which is not a probable process at all.

PL has been traditionally used to characterize the bulk-like properties of crystals; the light penetration depth is often in the range of 1 µm to 500 µm depending on the substrate material. However, PL is also sensitive to the surface (or interface) properties because the diffusion length of the excited electrons and holes can be several hundreds of nanometers. Although these excited carriers are mainly produced inside the bulk, they can easily reach the surface or interface parts by diffusing. The band-gap states at interface region play an important role in the intensity of the PL signal. The poor surface passivation can induce defect states at the energy bandgap therefore when the diffused electrons reach the surface part they recombine with the holes non-radiatively and ultimately cause the decrease in the PL intensity. Higher PL intensity means lower amount of defect states and reduction in the non-radiative recombination.

A typical PL experimental setup consist of light source, typically a LASER light which offers a monochromatic and collimated beam of light directed to the sample, optical lenses and filters and a photodetector.[54] A schematic diagram of PL experiment is shown in Fig 18.
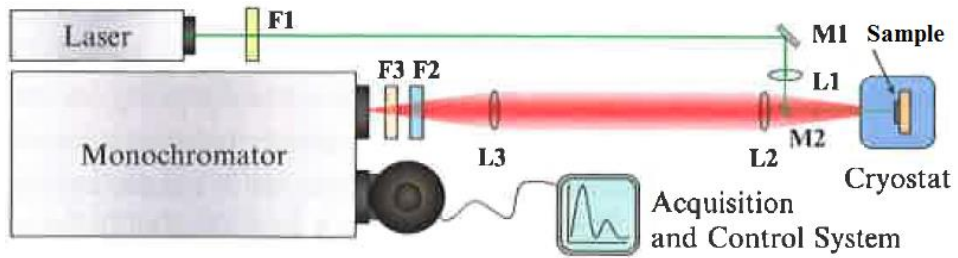
Figure18. Schematic representation of photoluminescence experimental setup, the symbols M, L and F are for mirror, lenses and filters, respectively. The figure is taken from ref. 54.

The peak wavelength of a PL spectrum tells the optical bandgap value of the bulk sample while the intensity of the spectrum is proportional to the density of photo excited electrons and, thus inversely proportional to the amount of non-radiative defects. If the interface region is not very well ordered then there is possibility of presence of trap states in the bandgap which increase the non-radiative recombination and decrease the PL intensity.
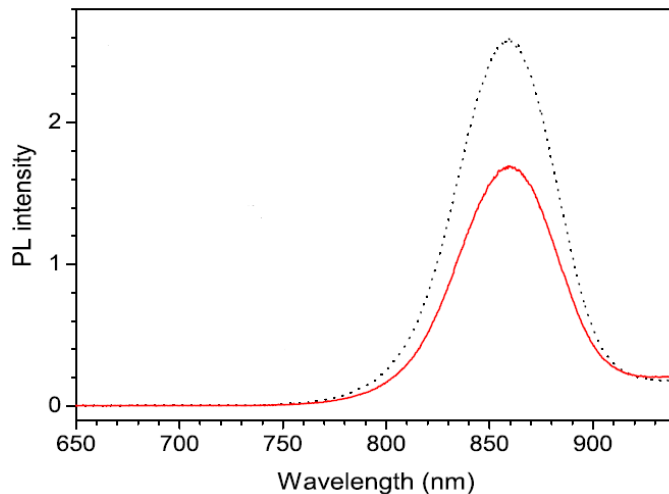

Figure 19. PL spectrum of Al2O3 shielded GaAs (100) sample with (dotted line) and without (solid line) passivation by BaO film.

In Fig. 19 a PL spectrum of GaAs sample is shown where the effect of BaO film deposition can be seen as an increase in the PL intensity or decrease in the interface defect densities.

3.5   Capacitance-Voltage (C-V) measurements

C-V measurement is another widely used electrical characterization method to study the oxide-semiconductor interface properties, for example, a gap-state density of metal oxide semiconductor (MOS) structure. A MOS structure can be considered as a capacitor where one electrode is gate-metal and other electrode is semiconductor substrate and both are separated by a thin metal-oxide insulating layer which acts as dielectric of the structure. A cross sectional diagram of MOS-capacitor is shown in Fig 20.

To perform the measurement and obtain a C-V curve, a DC biased voltage is applied across the gate and substrate, and then an AC- signal is superimposed on this signal. The response of capacitance as a function of varying DC bias, from negative to positive voltage,   is measured for MOS capacitor. The total capacitance of the MOS structure is dependent on the capacitance of oxide C_{ox} as well as the capacitance of semiconductor C_s, which can be considered making a series connection to each other.

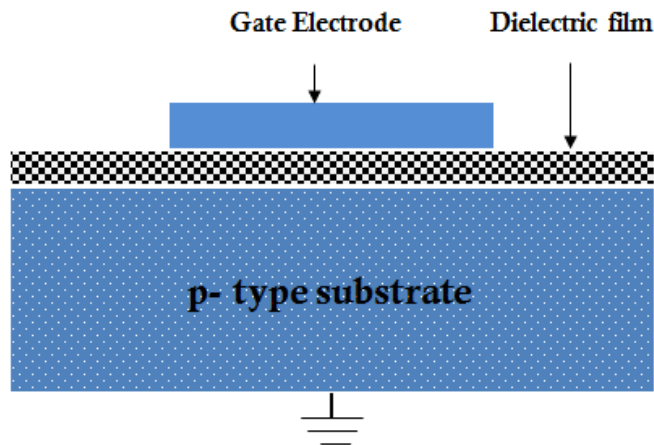Gate Electrode   Dielectric film

p- type substrate

Figure 20. Schematic diagram of p-type MOS structure.

In a p-type substrate, when the applied DC- signal achieves the negative value, the number of holes exponentially raises at oxide-semiconductor interface. This is the condition of accumulation and the total capacitance is based on oxide capacitance C_{ox}. With the decrease in the negative biased value, there starts forming a depletion region with a change in C_s which is added to the C_{ox}, and now the total capacitance is reduced because both capacitors are in series. At large positive bias voltage, the minority carriers (electrons in this case) move along to the interface and form the n-type inversion layer. At this stage again the total capacitance equals to the capacitance of oxide film C_{ox}, if the capacitance is measured at low frequency AC- signal (Fig. 21).
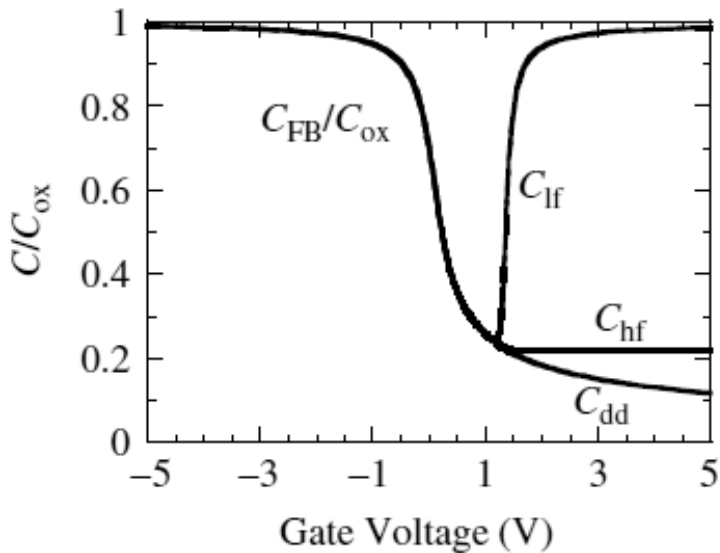

Figure21. A Capacitance- Voltage plot of an ideal p-MOS, showing the capacitance response curves of AC-signal frequency for low frequency, high frequency and deep-depletion. The figure is taken from ref. 55.

There is a time elapse of minority carrier to be generated, produce an inversion layer at interface and then recombine again after going back to substrate. This generation- recombination time is of the order of microseconds.[9] If we look at the Fig. 21, the C_{hf} correspond to the process where the frequency of the AC-signal is much higher than the generation-recombination time. At

very high frequency signal, there is no enough time for the formation of inversion layer and therefore the width of the depletion region keep increasing from its maximum position with the increase in the bias voltage and form a deep depletion region which further decreases the total capacitance. In Fig 21, this behavior is represented by C_{dd} curve.

The C-V curve can be used to measure the oxide film thickness d by using the C_{ox} value at the accumulation or in strong inversion region and also the permittivity of the material in the equation.

$$C_{ox} = \frac{\epsilon_{ox}}{d} \qquad (63)$$

where $'\epsilon_{ox}'$ is the permittivity constant for oxide film and $'d'$ is the thickness of the film.[9] The curve can also be used to find the substrate type; for example, a p- type substrate shows the large accumulation capacitance for the negative high frequency AC signals and a low capacitance for the positive voltages at high frequency signals. Opposite of this happens if the substrate is n-type.

The electrical properties of a MOS capacitor are largely determined by the properties of the oxide-semiconductor interface region. The C-V measurements together with simulations provide a quantitative analysis of the interface defect densities. In this thesis the quantitative analysis of CV curves is out of scope of our work therefore only qualitative interpretation of the interfaces is done with CV results. If the oxide-semiconductor interface contains a high density of the band-gap defects (let say more than 1×10^{15} cm^{-2}eV^{-1}), there would hardly be any capacitance modulation with the voltage change and the CV curve appear almost a straight line without any significant pit in the curve.
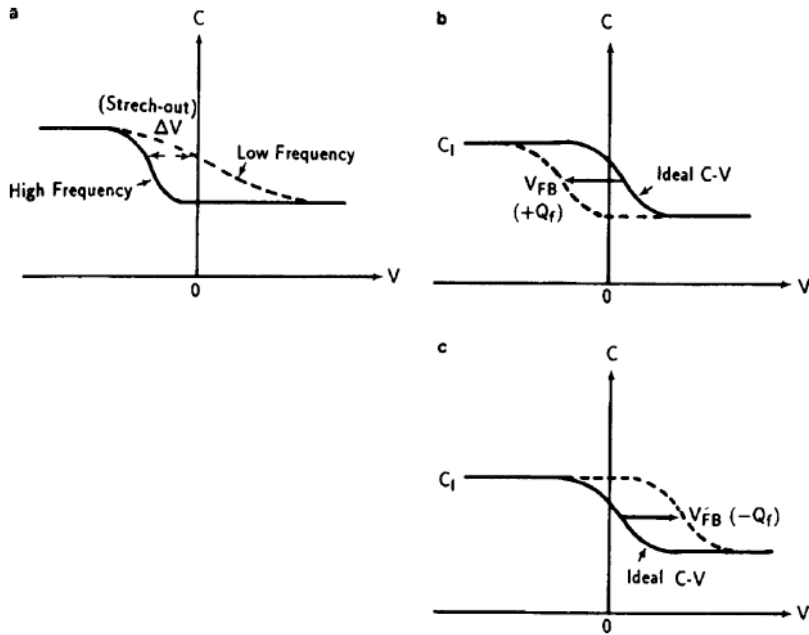
Figure22. Capacitance- Voltage plots of a p- MOS (a) At low frequency applied signal a stretching of curve is observed on voltage scale due to presence of interface trap densities at high frequency these states don't follow the signal therefore no significant change in the curve. (b) The shifting of C-V curve towards negative side of voltage axis due to presence of positive fixed oxide states. (c) If the negative fixed states present then the C-V plots move towards positive side of the voltage axis. The figure is taken from ref. 56.

When the AC signal is applied across MOS capacitor, the trap states are charged or discharged depending on the polarity of the signal. These states introduce an additional capacitance component as a result overall response of C-V curve is altered depending on the densities of these states. As it can be seen in Fig. 22a, these states don't follow the high frequency signal but at the lower frequency the C-V curve is stretched out on the voltage axis due to the presence of trap states. Also the presence of fixed oxide charges at oxide/ semiconductor interface introduce changes in the MOS behavior. These defect states arise during the oxide growth process and also depend on the orientation of silicon crystal and oxide annealing temperature. These states introduce a shift in the measured C-V plot from the ideal MOS. If the fixed oxide charges are positive then the shift will be towards negative biased (Fig. 22b) and opposite will be true if the fixed charges are negative (Fig. 22c). [12, 55-56]

4. Summary of results

4.1 Growth and properties of crystalline barium oxide on the GaAs (100) substrate. (Paper I)

Here we have addressed the question how the defect density can be decreased at the Al_2O_3/GaAs(100) interface. This junction is a prototypical example of the interface between an amorphous material (i.e., Al_2O_3) and the crystal. Such mismatch can generate point defects. The second problem has been a strong reactivity of GaAs with oxygen (i.e., GaAs surface oxidation). In Paper I, we have studied whether a thin crystalline barium-oxide film on GaAs(100) substrate can be used to control the Al_2O_3/GaAs(100) interface. We have utilized the PL, STM, STS and XPS characterization methods.

Two different GaAs samples were prepared after cleaning the crystal surfaces in UHV chamber by means of Ar –ion sputtering to remove the native oxides. One sample included an epitaxial BaO film on top of GaAs and the topmost Al_2O_3 cap on BaO, while the other sample was reference sample without the intermediate BaO film to compare the changes between two samples.

The BaO film was grown by means of thermal annealing of Ba metal which was angled normal to GaAs piece and was wrapped with the tungsten wire. The W coil was heated to evaporate Ba in presence of O_2 gas in the chamber in order to synthesize BaO film. The Al_2O_3 capping layer of about 3-4 nm was deposited by means of homemade ALD system on both of the samples for ex-situ measurements.

Before the growth of BaO film, a less than one monolayer Ba pre layer was deposited on top of GaAs piece to avoid the over oxidation of GaAs. The pre-layer was grown at room temperature, and it produced a GaAs(100)c(8×2)-

Ba reconstruction (Fig. 23a). The increase in the amount of Ba over 1 ML showed the Ba-nanolines structure.

The crystal quality of BaO was found to be sensitive to the ratio of Ba flux and O_2 pressure. To achieve a crystalline BaO film, a Ba flux of 0.5-1.0 ML/min was used with the oxygen partial pressure of $1-10\times10^{-7}$ mbar. The composition of the BaO film is calculated using the atomic sensitivity factors of both Ba and O and the Ba and O ratio is found 1:1 although the error calculation has not been performed. A (1×1) LEED pattern was appeared for 10-ML thick BaO film. Figure 23 shows the diffraction pattern as well as STM image of the 2D nature of BaO film. These results indicate crystalline nature for the grown BaO film. There is surely still room to improve the epitaxial nature of BaO, but for comparison, poor quality amorphous BaO films, which we grew during the iteration cycles, did not provide any LEED spot.
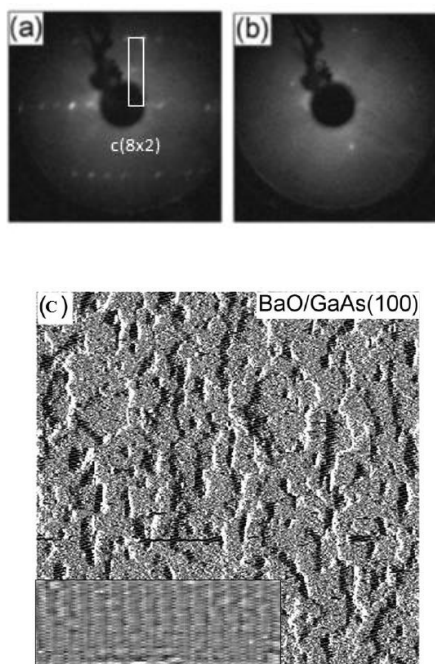

Figure 23. (a) A GaAs (100) *c*(8×2) reconstruction was produced after less than one ML of Ba pre-layer. (b) A (1×1) LEED patter confirms the crystalline quality of BaO film on GaAs (100) *c*(8×2)-Ba. (c) A STM image after 10-ML thick BaO film and inset shows the zoomed STM image of filled states of BaO film.

The comparison of PL spectra (Fig. 24) shows that there is significant advantage of BaO buffer layer. The higher GaAs peak intensity of PL for the sample containing BaO film is due to the improved oxide/GaAs interface with lowering of interface defects density because the samples are otherwise similar (i.e., the interface is only clear difference). A notable drop in the PL intensity was observed when the post heating temperature approached 700 ^{o}C which corresponds to degrading of oxide/GaAs junction. A clear shift in XPS measurement reveals the concomitant effect of heating: Ga3d peak shifts +1.5 or +2.0 eV for the samples heated at 700 ^{o}C, which corresponds to high-oxidation state of Ga due to diffusion of Ga atoms toward oxide film. The Ga diffusion is general problem when the oxide/GaAs junction is heated at elevated temperature. The PL spectra and XPS spectra can be seen in Fig. 24 (a) and Fig. 24 (b), respectively.
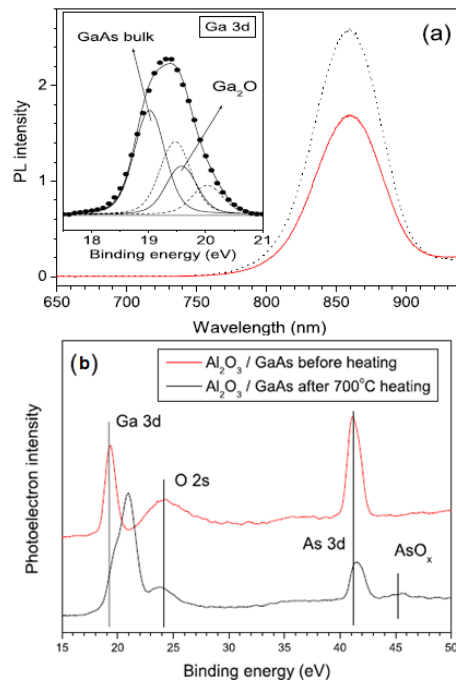

Figure 24. (a)A comparison between PL spectra of samples with (dotted line) and without BaO (solid line) buffered layer clearly indicates the high intensity of PL for buffered sample. The inset represents the Ga3d spectrum for Al$_2$O$_3$/GaAs. (b) The effect of heating when sample was heated at 700 ^{o}C induce the diffusion of Ga atom into the oxide film and degrade the interface quality.

4.2. Atomic structure and thermally induced transformation of crystalline BaO/Si(100) junction. (Paper II)

In Paper II, we studied the properties of the BaO/semiconductor interface in more detail by measuring an epitaxial BaO/Si(100) junction by means of synchrotron photoemission spectroscopy. A model is constructed for the BaO/Si interface on the basis of the measurements as a function of the post-growth heating of the sample up to 500 $^{\circ}$C.

The (100) surfaces of Si crystals were cleaned by rapid flash heating in UHV. After cleaning the Si surface was covered with 0.5 ML of Sr atoms at RT and annealed afterwards at 530-660 $^{\circ}$C before deposition of BaO film. The electropositive Sr atoms donate electrons to the surface atoms which saturate the Si dangling bonds and symmetrize the Si dimers. The Ba and Sr evaporators were made by circulating the tungsten wire around the metals. The BaO film was deposited at RT on Sr covered Si(100) using the oxygen background pressure of 8×10^{-8} Torr and a Ba flux of ~0.65-0.7 ML/min.

LEED pattern shows the (1×2) periodicity after Sr deposition. On top of this structure, BaO film was deposited via thermal evaporation of Ba metal under oxygen pressure at room temperature. The film thickness was expressed according to the amount of deposited Ba therefore, e.g., the 2ML BaO means that the film is grown by depositing 2ML Ba in the oxygen environment. The Ba deposition rate was calibrated with LEED by observing the previously established and documented phase diagram of the Ba/Si(100) as a function of Ba deposition time and substrate temperature.[57]

The results show that the (1×2)- Sr periodicity was intact up to 2ML deposition of BaO but vanishes when 5 ML of BaO was grown, and is replaced by (1×1) periodicity which was not changed even when the BaO coverage was 25 ML.

To understand the interface structure, a comparison of core level shifts (CLS) in Si 2p spectra was performed for Silicon samples with (1×2) – Sr, SiO₂/Si, 2ML BaO and 5 ML BaO with and without heating at elevated temperature which are shown in the Fig. 25.
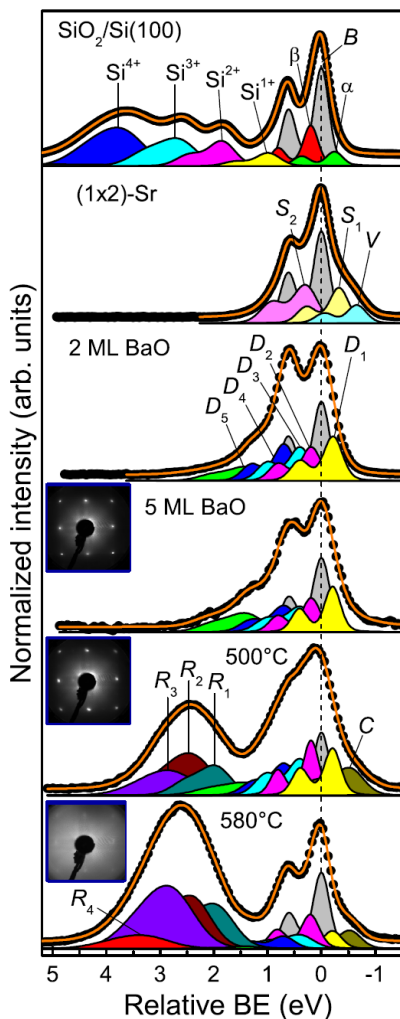

Figure 25. Si 2p core level spectra of SiO2/Si, (1×2)- Sr and 2 ML and 5 ML BaO/Si with and without annealing at elevated temperatures.

To identify the origins of the different components the measured CLS was compared with the predicted CLS for different Sr(Ba)-Si-O bonding configurations shown in Fig. 26 (a). The well-studied system of SiO_2/Si is used

for the prediction, where Si atoms with different oxidation states could be surrounded by different number of oxygen atoms. In SiO_2/Si case, the CLS corresponding to each of the bonding configurations (top row of Fig. 26 (a)) are very well known. On the other hand, the Sr/Si(1x2) interface which is the simplest case where top Si atoms interact with Sr atom and give rise a S_1 component (-0.33eV). Combining the information of both the SiO_2/Si and the Sr/Si(1x2) systems, the resulted binding energy shifts of the other metal-Si-O configurations are assumed. The comparison of predicted and measured CLS reveals that the D_1 and D_2 are originated from those interfacial Si atoms which are not bonded to the oxygen atoms. The components D_3-D_5 are originated from Si surrounded either by one O atom and two metallic atoms or two O atoms but one metallic atom but no more than two bonds with O atoms but not from Si-Si bonding or Si metal bonding. Using this analysis, a model of atomic structure of BaO/Si interface is suggested which is shown in Fig. 26 (b).
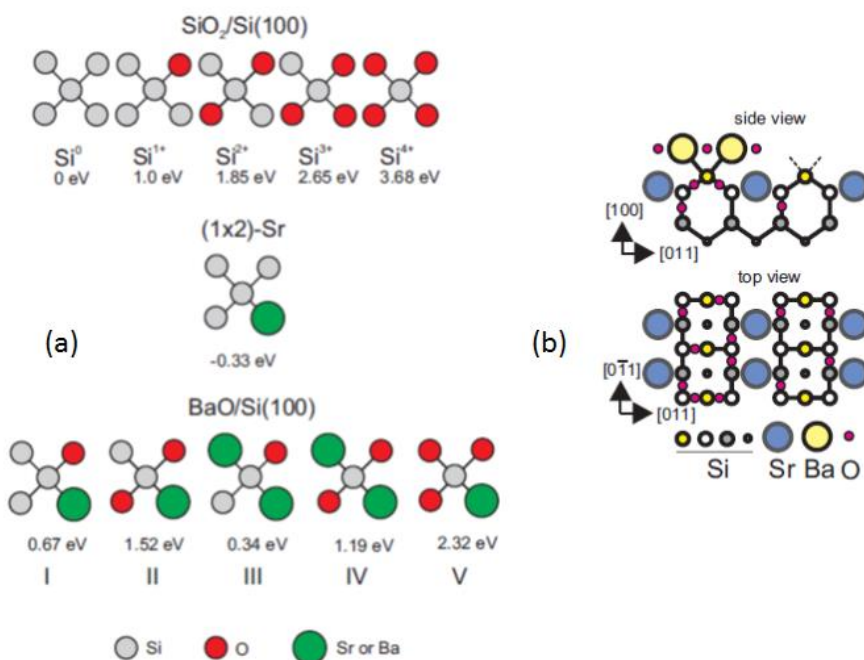

Figure 26. (a) Predicted bonding configuration and corresponding CLS values for Si 2p. (b) Suggested model of atomic structure BaO/Si interface.

When compared to the previous atomic models of BaO/Si,[58] our findings show that the BaO/Si interface becomes oxidized more than expected previously and results in more complicated interface region. It is assumed in this model that the oxygen atoms are incorporated randomly with Si atoms in at least three upper most Si layers. It is interesting that the interface still remains highly crystalline, despite of the increased Si-O bonding and it is in good agreement with the resulting D_3-D_5 components in Si 2p spectrum. Since the Si 2p core level spectra for 2ML and 5 ML BaO/ Si are rather similar and include same interface related components, it can be safely assumed that the interface is not considerably affected with film thickness and it can also be concluded that the Sr-covered Si surface starting surface is a good platform to grow BaO film.

The stability at elevated temperature was examined when the 5 ML BaO/Si sample was annealed at 500 ^{o}C. LEED confirms the epitaxial film but Si 2p spectrum shows high binding energy components R1-R3 which are resulted due to diffusion of Si atoms toward BaO film, resulting in O-rich bonding environment. Further annealing at 580°C affected notably to the crystalline BaO film and transformed the film amorphous. The heating durability is an important aspect when the epitaxial growth of the second film (e.g., III-V compound semiconductors) is considered on the top of BaO/Si(100). The key finding of the experiment is the penetration of oxygen up to 4 Si layers without disturbing the crystallinity of the film and also the interface region is not that straight forward as it was previously found.[58]

4.3. Observation of unusual metal-semiconductor interaction and metal-induced gap states at an oxide-semiconductor interface: The case of epitaxial BaO/Ge(100) junction. (Paper III)

Paper III presents a continuation of the studies of BaO/semiconductor interfaces. The BaO/Ge junction provides a potential template to elucidate the interaction of Ba and a semiconductor because the Ge-O interaction is clearly weaker than for Si-O and GaAs-O. The obtained results give an evidence for that the bandgap defect states at the interface arise from the Ba-Ge reaction which is not usual because these defect states have been usually considered to arise from the oxygen-semiconductor interaction.

Two Ge samples were prepared for BaO film growth, namely; type-1 and type-2. In type-1 sample, BaO was grown on clean Ge with (2×1) dimer rows while in type 2 sample, a pre-layer of Ba was deposited on clean Ge to remove surface dangling bonds before the deposition of BaO film. This leads to $c(4\times4)$ reconstruction. Then the c(4x4) was exposed to oxygen at RT to form the (1x2) structure stabilized by both Ba and O. BaO film was grown on both substrates, and such films show the same (1×1) LEED pattern, which indicates that film crystallinity is not dependent on the type of the samples. However, in spite of such a similarity, the interface properties are not identical in the two systems at all, as it will be described below.

Comparison of the valence band spectra of both samples shows a clear difference in the position of Fermi level and also the appearance of band bending. Since in both samples the deposited film was crystalline but the starting surface was different therefore some changes in the interface region were expected. To understand the differences, the core level spectroscopy of Ge was performed and it was found in CL spectra that the main difference is the

number of Ba-induced defects which are assumed based on the shift of corresponding peak. These defects were considered to be the responsible of the band bending. In addition to this, CL spectra show that there is no Ge oxide. It leads to the conclusion that the interaction of Ba atoms rather O atoms affects the BaO/Ge interface which is unusual. These defect states can be controlled by surface modification of Ge before the deposition of oxide film.
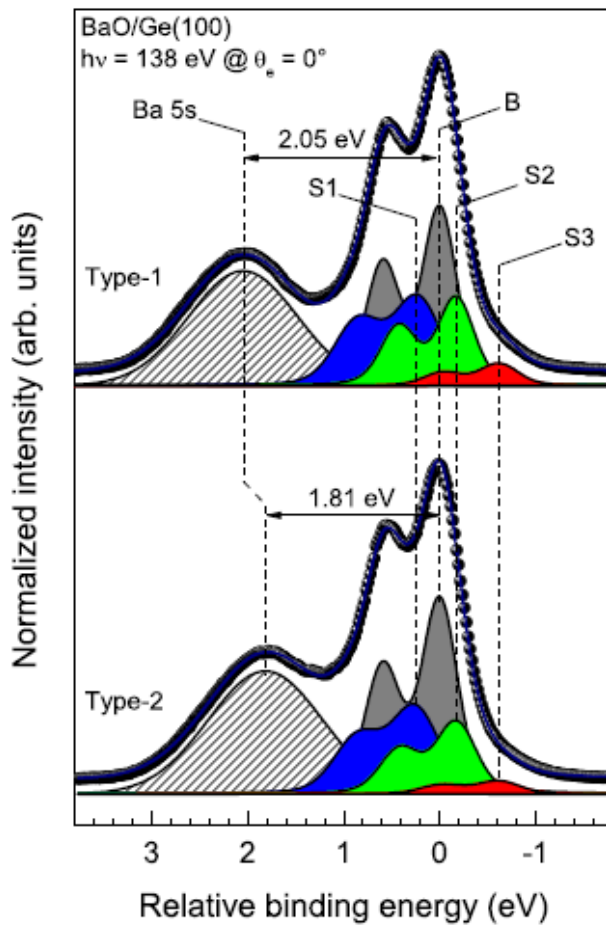

Figure27. The Ge 3d core level spectra of both type 1 and type 2 BaO/Ge samples that represent the different shifted component.

4.4. Towards the atomically abrupt interfaces of SiO$_x$ / semiconductor junctions (Paper IV)

From the results of Papers I-III, we learned that the interaction of a semiconductor crystal with both oxygen and non-oxygen elements of a metal-oxide film should be avoided in order to decrease the amounts of interface defects. Furthermore, it has been known that the cleaning of semiconductor wafer surfaces in scalable manner is not straightforward. These issues motivated us to study an alternative method to produce oxide-semiconductor junction.

Paper IV presents the evidence of non-oxygen element induced degradation in insulator/semiconductor interface. Two steps procedure is suggested to avoid this degradation. 1) Synthesis of metallic film on naturally oxidized semiconductor surface and 2) Proper consideration of post annealing temperature for growth of insulating film. The semiconductor substrates used in this research includes Ge (100) and GaInAs (100) and insulator/semiconductor junctions were studied after deposition of SiO$_2$ or SiO$_x$N$_y$ film on these substrates. Harmful effects due to silicon-substrate interaction were evident by means of PL, C-V and XPS measurements.

Using GaInAs substrate three samples were prepared 1) Al$_2$O$_3$/SiN$_x$/GaInAs sample where an intermediate SiN$_x$ film was deposited before Al$_2$O$_3$ film on GaInAs sample. 2) Al$_2$O$_3$/GaInAs (as reference sample I) on clean GaInAs (100) after removing of As cap layer. 3) As/GaInAs (reference sample II) substrate without any treatment and removal of As cap layer from substrate. The comparison of PL spectra (Fig. 28), clearly shows the higher intensity of reference sample Al$_2$O$_3$/GaInAs. The lower intensity of Al$_2$O$_3$/SiN$_x$/GaInAs indicates an increase in the electronic defects density which is due to strong interaction of Si with GaInAs sample.

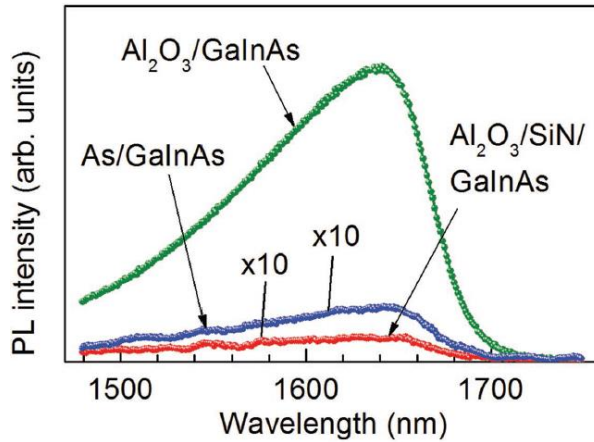Figure 28. Comparison of PL spectra of Al$_2$O$_3$/SiN$_x$/GaInAs with reference samples Al$_2$O$_3$/GaInAs, As/GaInAs.

These results were further tested using Ge system. Two Ge (100) samples were prepared by using two different synthesis methods of SiO$_2$ film deposition. The reference sample was prepared using the conventional method, where SiO$_2$ film was grown using by first depositing pure Si film clean Ge(100)(2×1) and then the substrate is oxidized. For other sample, a novel method was developed and tested to synthesize the same 2-nm SiO$_2$ film. In this method no prior cleaning of Ge sample was performed and pure Si was deposited on this naturally oxidized Ge sample which was then followed by post heating. In the CV measurements, the clear differences in the capacitance modulation indicate that the Si film growth on oxidized Ge has better interface and it is inferred that harmful diffusion of Si into Ge sites are the cause of degradation of electrical properties for samples where SiO$_2$ was deposited on clean Ge using conventional method.

A detailed study of atomic environment at the interface region for Si/GeO$_x$/Ge sample was performed using PES measurements. Fig. 29 shows the comparison of both Ge-3d and Si- 2p core-levels for Si-covered GeO$_x$/Ge with GeO$_x$/Ge and SiO$_2$/Si samples, respectively. It was found that Si deposition on oxidized Ge removes the two components Ge^{1+} and Ge^{2+} which correspond to

the transfer of oxygen from germanium to silicon and results sharp SiO_2/Ge interface with less defect states, more uniform SiO_2 film stoichiometry with dominancy of SiO_2 character.
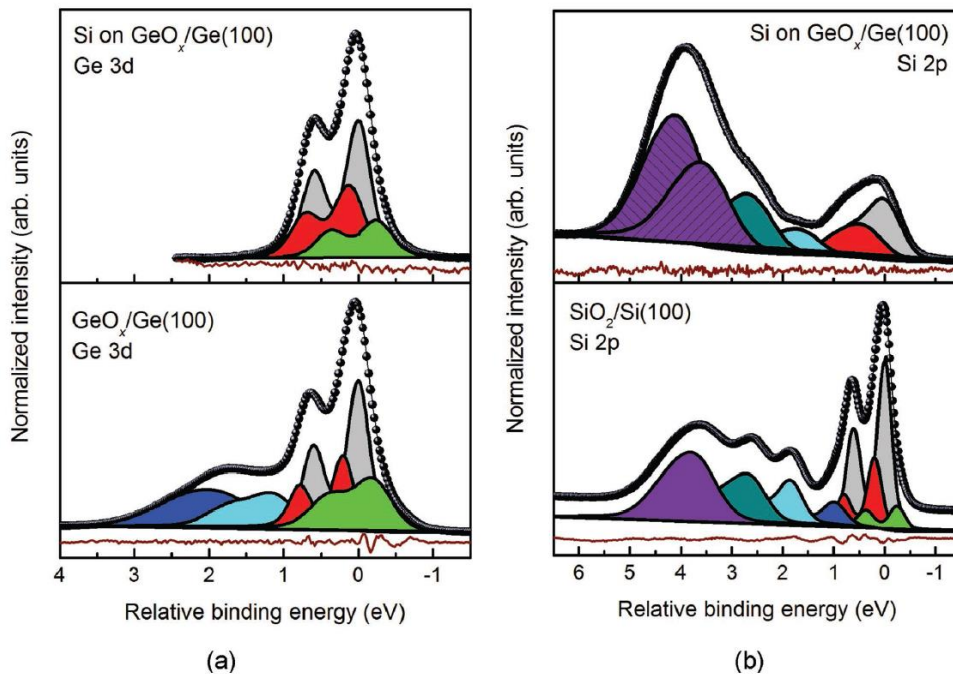

Figure 19. (a) Ge 3d core-level spectra for Si/GeO$_x$/Ge and GeO$_x$/Ge. (b) Si 2p core-level spectra of Si/GeO$_x$/Ge and SiO$_2$/Si

To investigate the structure of oxide film, a comparison of Si 2p spectra for SiO_2/Si and Si/GeO$_x$/Ge was performed which is shown in Fig. 19b. A key finding in the Si 2p spectrum for Si-covered GeO$_x$/Ge system was the changes in the oxidation states of Si (Si^{1+}, Si^{2+}, Si^{3+} and Si^{4+}). For example, a commonly found Si-oxide related bonding site Si^{1+} was not present in the Si 2p spectrum for Si/GeO$_x$/Ge, beside this the intensities of other oxide related components Si^{2+} and Si^{3+} were relatively low compared to same components in SiO_2/Si system. On the other hand, the significantly large intensity corresponding to Si^{4+} species was observed in the Si/GeO$_x$/Ge system. This further confirms the

presence of a uniform stoichiometry of the oxide film deposited via the novel method compared to traditional synthesis method.

4.5. Synthesis and properties of crystalline thin film of antimony trioxide on the Si (100) sample. (Paper V)

In Paper V, a simple method for the preparation of single crystalline thin film of antimony trioxide (Sb_2O_3) is demonstrated on clean Si(100) substrate. The film analysis was performed by means of LEED, STM and STS. The ab initio density functional theory (DFT) is used to calculate the surface atomic models and corresponding STM simulated images.

The clean Si(100) is used to perform the synthesis of different amount (1-5 nm) antimony (Sb) film. There appeared clusters of Sb on Si sample which was removed after the film oxidation with O_2 pressure of 3-4 $\times 10^{-6}$ mbar. Fig. 30 represents the cluster formation and removal of cluster upon oxidation for 5 nm thick Sb film.
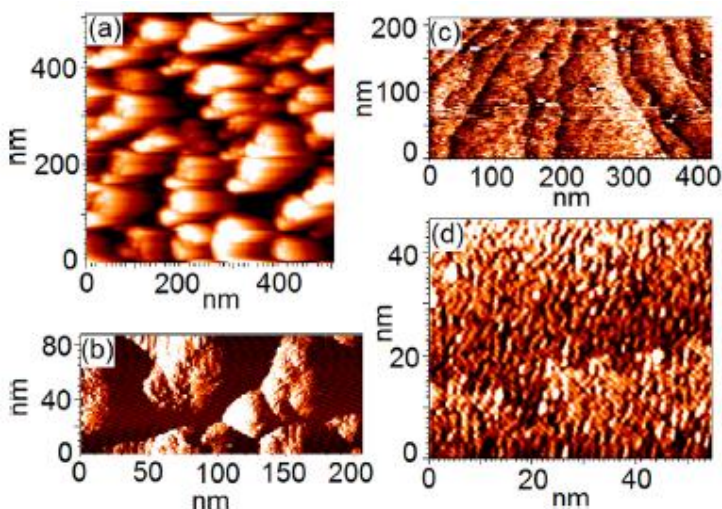

Figure 30. The Sb clusters (a) and (b) disappeared (c) and (d) after the oxidation was performed with the substrate temperature of 500 °C for 5nm thick film of Sb.

It is found that the substrate temperature and the oxidation time are two crucial parameters for smooth and crystalline Sb_2O_3 film. A good quality two

dimensional Sb_2O_3 film with Sb/O ratio of 0.7 was obtained when the substrate temperature was 500 $^{\circ}$C and oxidation time is 20-50 min (depends on the thickness of initial Sb film). The (1×1) pattern, appeared in LEED, confirms the crystallinity of film structure. The film was partially oxidized when the oxidation was performed for substrate temperature below 500 $^{\circ}$C (for example 450 $^{\circ}$C). For substrate temperature above 500 oC the film degradation was started.

There are 5 different surface models of Sb_2O_3 film were calculated and corresponding theoretical STM images for both empty and filled states were simulated. These model include Sb_2O_3 (111), Sb_2O_3 (100)-1, Sb_2O_3 (100)-2, Sb_2O_3 (100)-3, Sb_2O_3 (100)-4. On the basis low surface energy values, two of the models Sb_2O_3 (100)-2 and Sb_2O_3 (100)-4 were found more appropriate. The comparison between measured STM images and theoretical STM images was also in agreement with these two models.

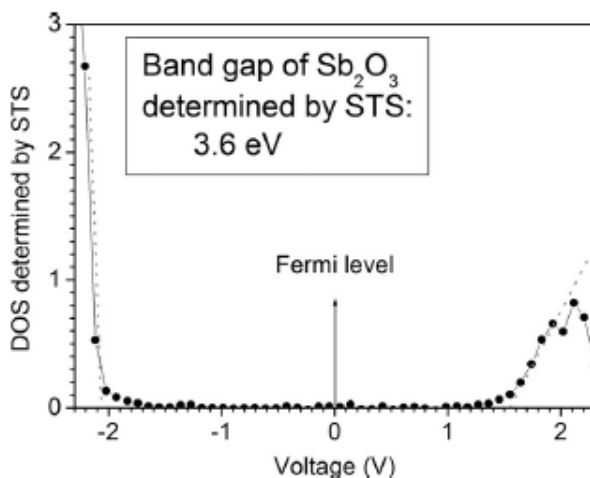**Figure 31. The STS spectrum shows the band gap (i.e ~3.6 eV) of the film and also that the film is slightly n-doped because the Fermi level positon is rather close to conduction band.**

The STS measurements (shown in Fig. 31) reveal the surface bandgap of the film and it was found that the bandgap of Sb_2O_3 film is 3.6 ± 0.1eV and the film is slightly n-doped.

5. Concluding remarks

The thesis comprises the growth and characterization of the different junctions formed by a metal-oxide film on a semiconductor crystal. The main motivation has been to find potential solutions to decrease the amounts of defects at the metal-oxide/semiconductor interfaces, which are harmful to the operation of various electronics devices like transistors and solar cells. Our approach is based on the surface-science knowledge and methods.

The first three studies were focused on the epitaxial BaO films on the GaAs(100), Si(100), and Ge(100) substrates, respectively. This epitaxial BaO interface layer was found to decrease the defect amount of the Al_2O_3/GaAs junction. For BaO/GaAs, a metallic pre-layer of Ba, before the oxide growth, showed an atomic ordering or crystal nature, and turned out to be very useful to protect the interface against harmful oxidation during the BaO growth. In order to advance the understanding of physical and chemical properties of BaO/semiconductor junctions, we have utilized the synchrotron-radiation PES, which enables the characterization of bonding environments at the buried interface with high resolution. The results indicate that a great care should be addressed to control of the semiconductor reaction with both oxygen and metal elements.

In BaO/Si structure, the oxygen atoms were found to be incorporated into the Si planes up to four Si atomic planes, keeping still the crystallinity of the material. On the basis of these results an atomic model is also proposed for BaO/Si system.

It was evident for the BaO/Ge system that the band gap defect states in the oxide/semiconductor junction were not formed by usual oxidation of semiconductor surface but due to the interaction of Ba metal with semiconductor substrate. These states results the pinning of Fermi- level

position and also cause the band bending. These electronic states can be suppressed by careful modification of initial Ge surface before deposition of oxide film.

The harmful metal-semiconductor interaction is observed when the SiO_2 was deposited on semiconductor substrate (Ge and GaAs). It is presented that how this degradation can be avoided using an improved method of deposition of SiO_2 film on Ge(100) and GaAs(100). It is found that a good quality oxide/semiconductor interface can be tailored if SiO_2 is grown by deposition of Si layer on oxidized Ge(100) or GaAs(100) with proper consideration of post-heating temperature.

Crystalline Sb_2O_3 film is synthesized with the careful adjustment of temperature and oxidation time. The two-dimensional film is evident in the measured STM images. The theoretically calculated STM images by means of DFT calculation are well matched with the measured STM images. The STS data also supports the film uniformness and therefore successfully reviled the film bandgap.

In future, it is interesting to transfer the above results to device tests and also compare the experimental findings with computational results.

References

[1] Niklas Nilius. Properties of oxide thin films and their adsorption behavior studied by scanning tunneling microscopy and conductance spectroscopy. Surface Science Reports. 2009. 595-659.

[2] Jian Wang, Low Energy Electron Diffraction Studies of Transition Metal Oxide Surfaces and Films, PhD Dissertation.

[3] R. M. Wallace and G. D. Wilk, Crit. Rev. Solid State **28**, 231 (2003).

[4] P.Zubko, S. Gariglio, M. Gabay, P. Ghosez and Jean-Marc Triscone. Interface Physics in Complex Oxide Heterostructures. Annu. Rev. Condens. Matter Phys. 2011. 141-165.

[5] W. A. Doolittle, A. G. Garver and W. Henderson, Molecular beam epitaxiy of complex metal-oxides: where have we come, where are we going, and how are we going to get there?. Journal of Vacuum Science and Technology B, vol. 23(3), pp. 1272-1276, 2005.

[6] R. A. McKee, F. J. Walker and M. F. Chisholm, Physical Structure and Inversion, Science, pp. 468-471, 2001.

[7] T. L. Goodrich, J. Parisi, Z. Cai, and K. S. Ziemera. Low temperature growth of crystalline magnesium oxide on hexagonal silicon carbide (0001) by molecular beam epitaxy. Applied Physics Letters 90, 042910 (2007).

[8] Tuomo Suntola. Atomic layer Epitaxi. Thin solid films 216 (1992). 84-89.

[9] D. T. Hawkins. Chemical vapor deposition, A bibliography, Plenum, New York, 1999.

[10] A. Y. Cho, J. R. Arthur. Molecular beam Epitaxi. Progress in solid-state chemistry. 1975. 157-191.

[11] Pulsed Laser Deposition of Thin Films, edited by Douglas B. Chrisey and Graham K. Hubler, John Wiley & Sons, 1994.

[12] Ben G. Streetman and Sanjay Banerjee. Solid State Electronic Devices. 6th Edition. (2009).

[13] S. M. Sze, M. K. Lee. Semiconductor Devices Physics and Technology. 3rd edition.

[14] Marja Ahola- Tuomi. Unusal bismuth- containing surface layers of III- V compound Semiconductors. PhD Dissertation.

[15] Jouko Lång. Research and Development of III-V Semiconductor Surfaces for Improved Device Interfaces. PhD Dissertation.

[16] Charles B. Duke. Semiconductor Surface Reconstruction: The structural chemistry of two-dimensional surface compounds. Chem. Rev. 1996, 96, 1237-1259.

[17] Theory of semiconductor surface reconstruction. G. P. Srivastava. Rep. Prog. Phys. 60 (1997). 561-613.

[18] Chih-Tang Sah. Fundamental of solid state electronics.

[19] L.G. Meiners and H.H. Wieder. Semiconductor surface passivation. Materials Science Reports 3 (1988) 139-216.

[20] Chopra, K. Major, S. Pandya, D. Transparent conductors- A status review. Thin Solid Films 1983, 102, 1–46.

[21] David S. Hecht , Liangbing Hu , and Glen Irvin. Emerging Transparent Electrodes Based on Thin Films of

Carbon Nanotubes, Graphene, and Metallic Nanostructures. Adv. Mater. 2011, 23, 1482–1513.1

[22] Ronglei Fan, Jiawei Min, Yian Li, Xiaodong Su, Shuai Zou, Xusheng Wang and Mingrong Shen. n-type silicon photocathodes with Al-doped rear p+ emitter and Al2O3-coated frontsurface for efficient and stable H2 production. App. phys. let. 106, 213901 (2015).

[23] J. W. Reiner, A. M. Kolpak, Y. Segal, K. F. Garrity, S. Ismail-Beigi, C. H. Ahn, and F. J. Walker, Adv. Mater. 22, 2919 (2010).

[24] S. A. Chambers, Adv. Mater. 22, 219 (2010).

[25] F. J. Himpsel, K. N. Altman, J. N. Crain, A. Kirakosian, J.-L. Lin, A.Liebsch and V. P. Zhukov. Photoelectron Spectroscopy of atomic wires. J. Electron Spectrosc. Relat. Phenom. 2002. 89-99.

[26] Hans-Joachim freund, H. Kuhlenbeck and V. Staemmler. Oxide Surfaces. Rep. Prog. Phys. 1996. 283-347.

[27] M. D. Pashley. Electron counting model and its application to island structures on molecular-beam epitaxy grown GaAs(001) and ZnSe(001) . Phys. Rev. B, vol. 40, number 15, 10481-10487.

[28] https://en.wikipedia.org/wiki/Surface_reconstruction.

[29] M. Yasir, J. Dahl, M. Kuzmin, J. Lång, M. Tuominen, M. P. J. Punkkinen, P. Laukkanen, K. Kokko, V.-M. Korpijärvi, V. Polojärvi, and M. Guina. Growth and properties of crystalline barium oxide on the GaAs(100)

substrate. Applied Physics Letters 103, 191601 (2013).

[30] M. Yasir, M. Kuzmin, M.P.J. Punkkinen, J. Mäkelä, M. Tuominen, J. Dahl,P. Laukkanen, K. Kokko. Synthesis and properties of crystalline thin film of antimony trioxide on the Si(1 0 0) substrate. Applied Surface Science 349 (2015) 259–263.

[31] J. E. A. M. van den Meerakker and M. H. M. van der Straaten. A Mechanistic Study of Silicon Etching in NH_3 / H_2O_2 Cleaning Solutions. J. Electrochem. Soc. 1990 137(4): 1239-1243.

[32] P. Laukkanen, M. Kuzmin, R.E. Perälä, R.-L. and Vaara, I.J. Väyrynen. Scanning tunneling microscopy study of GaAs(1 0 0) surface prepared by HCl-isopropanol treatment. Applied Surface Science 206 (2003) 2-7.

[33] C. C. Cheng, K. V. Guinn, I. P. Herman, and V. M. Donnelly. Competitive halogenation of silicon surfaces in HBr/Cl2 plasmas studied with x-ray photoelectron spectroscopy and in situ, real-time, pulsed laser-induced thermal desorption. J. Vac. Sci. Technol. A 13(4), Jul/Aug 1995.

[34] Richard W. Johnson, Adam Hultqvist and Stacey F. Bent. A brief review of atomic layer deposition: from fundamentals to applications. Materials Today. Volume 17, number 5, June 2014.

[35] http://cnx.org/contents/ae29812b-5c71-4740-ac36-6809c5282026@2/Atomic-Layer-Deposition

[36] Mahboubeh Hotamani. Theory of Adsorption, Diffusion and Spinpolarization of Mn on Si(001) and Si(111) Substrates, PhD Dissertation.

[37] John C. Vickerman and Ian S. Gilmore. "Surface Analysis the principle technique". 2nd Edition.

[38] https://www.uni-marburg.de/fb13/researchgroups/molecular-solid-state-physics/methods/methods_leed?language_sync=1.

[39] J. J. K. Lång, M. P. J. Punkinen, M. Tuominen, H. –P. Hedman, M. Vähä-Heikkilä, V. Polojärvi, J. Salmi, V. – M. Korpijärvi, K. Schulte, M. Kuzmin, M. Guina, K. Kokko, R. Punkkinen, and P. Laukkanen. Atomic scale engineering of oxide/semiconductor interface for improved transistors.

[40] Pekka Laukkanen. Atomic and Electronic properties of GaAs (100) and InAs (100) semiconductor surfaces. PhD Dissertation. 2005.

[41] Hafiz Muhammad Sohail. Experimental and theoretical studies of metal adsorbates interacting with elemental semiconductor surfaces. PhD Dissertation. Linköping University. 2014.

[42] Justin Bogan. Growth and chemical characterization studies of Mn silicate barrier layers on SiO2 and CDO. PhD Dissertation. Dublin city university (2012).

[43] A. Zangwill, Physics at Surfaces, Cambridge University Press, (1988).

[44] P. E. J. Eriksson and R. I. G. Uhrberg, Surface core-level shifts on clean Si(100) and Ge(100) studied with photoelectron spectroscopy and density functional theory calculations. Physical Review B 81, 125443 (2010).

[45] E. Landermark, C. J. Karlsson, Y. –C. Chao and R. I. G. Uhrberg, Core- level spectroscopy of the clean Si(100) surface: charge transfer within asymmetric dimers of the 2 x 1 and c(4 x 2) reconstructions. Physical Review Letters 69 (1992).

[46] Johnny Dahl. Spectroscopic studies of III-V semiconductor material for improved devices. PhD Dissertation. 2015.

[47] D. A. Shirley, Phys. Rev. B 5, 4709 (1972).

[48] Martin Hjort. Surface studies of III-V nanowires. Lund University, Sweden (2012).

[49] Riikka-Liisa Vaara. Rare-earth-metal-induced nanoscale structures on Si(111) surface studied by scanning tunneling microscope and low-energy electron diffraction. University of Turku (2004).

[50] Joakim Hirvonen. Thin Mn silicide and germanide layers studied by photoemission and STM. Karlstad University (2012).

[51] , J. Mäkelä, M. Tuominen, M. Yasir, M. Kuzmin, , J. Dahl, M.P.J. Punkkinen, P. Laukkanen, K. Kokko, R. M. Wallace. Oxidation of GaSb (100) and its control studied by scanning tunneling microscopy and spectroscopy. Applied Physics Letters 107, 061601 (2015).

[52] J. Bardeen, Phys. Rev. Lett. 6 (2), 57- 59 (1961).

[53] J. Tersoff, and D. R. Hamann, Phys. Rev. B 31, 805 (1985).

[54] Semiconductor Research: Experimental Techniques, edited by Amalia Patané and Naci Balkan, Springer (2012).

[55] D. K. Schroder. Semiconductor Material and Devices Characterization, 3rd Edition, John Wiley & Sons Inc. (2006).

[56] Sheng S. Li. Semiconductor Physical Electronics, Springer (2006).

[57] Xiaoming Hu, Z. Yu, J. A. Curless, R. Droopad, K. Eisenbeiser, J. L. Edwards Jr., W. J. Ooms and D. Sarid. Comparative study of Sr and Ba adsorption on Si (100). Applied Surface Science 181 (2001) 103- 110.

[58] Y. Segal, J. W. Reiner, A. M. Kolpak, Z. Zhang, S. Ismail-Beigi, C. H. Ahn, and F. J. Walker. Phys. Rev. Lett. 102, 116101. (2006).

[59] E. Landemark, C. J. Karlsson, Y.-C. Chao and R. I. G. Uhrberg. Core- level spectroscopy of the clean Si(001) surface: Charge transfer within Asymmetric dimers of the 2×1 and c(4×2) reconstruction.